Published in final edited form as:
Atmos Environ (1994). 2021 June 1; 254: . doi:10.1016/j.atmosenv.2021.118371.

Impact of various air mass types on cloud condensation nuclei concentrations along coastal southeast Florida

Eva-Lou Edwards[a], **Andrea F. Corral**[a], **Hossein Dadashazar**[a], **Anne E. Barkley**[b], **Cassandra J. Gaston**[b], **Paquita Zuidema**[b], **Armin Sorooshian**[a,c,*]

[a] Department of Chemical and Environmental Engineering, University of Arizona, Tucson, AZ, USA

[b] Rosenstiel School of Marine and Atmospheric Science, University of Miami, Miami, FL, USA

[c] Department of Hydrology and Atmospheric Sciences, University of Arizona, Tucson, AZ, USA

Abstract

Coastal southeast Florida experiences a wide range of aerosol conditions, including African dust, biomass burning (BB) aerosols, as well as sea salt and other locally-emitted aerosols. These aerosols are important sources of cloud condensation nuclei (CCN), which play an essential role in governing cloud radiative properties. As marine environments dominate the surface of Earth, CCN characteristics in coastal southeast Florida have broad implications for other regions with the added feature that this site is perturbed by both natural and anthropogenic emissions. This study investigates the influence of different air mass types on CCN concentrations at 0.2% ($CCN_{0.2\%}$) and 1.0% ($CCN_{1.0\%}$) supersaturation (SS) based on ground site measurements during selected months in 2013, 2017, and 2018. Average $CCN_{0.2\%}$ and $CCN_{1.0\%}$ concentrations were 373 ± 200 cm^{-3} and 584 ± 323 cm^{-3}, respectively, for four selected days with minimal presence of African dust and BB (i.e., background days). CCN concentrations were not elevated on the four days with highest influence of African dust (289 ± 104 cm^{-3} [0.2% SS] and 591 ± 302 cm^{-3} [1.0% SS]), consistent with high dust mass concentrations comprised of coarse particles that are few in number. In contrast, CCN concentrations were substantially enhanced on the five days with the greatest impact from BB (1408 ± 976 cm^{-3} [0.2% SS] and 3337 ± 1252 cm^{-3} [1.0% SS]). Ratios of $CCN_{0.2\%}$:$CCN_{1.0\%}$ were used to compare the hygroscopicity of the aerosols associated with African dust, BB, and background days. Average ratios were similar for days impacted by African dust and BB (0.54 ± 0.17 and 0.55 ± 0.17, respectively). A 29% higher average ratio was observed

* Corresponding author. Harshbarger Building, 108, PO Box 210011, Tucson, AZ, 85721-0011, USA. armin@email.arizona.edu (A. Sorooshian).

CRediT authorship contribution statement

Eva-Lou Edwards: Conceptualization, Methodology, Software, Formal analysis, Writing – original draft, Visualization. **Andrea F. Corral:** Conceptualization, Methodology, Writing – review & editing. **Hossein Dadashazar:** Software, Writing – review & editing. **Anne E. Barkley:** Investigation, Resources, Data curation, Writing – review & editing. **Cassandra J. Gaston:** Investigation, Resources, Data curation, Writing – review & editing. **Paquita Zuidema:** Investigation, Resources, Data curation, Writing – review & editing. **Armin Sorooshian:** Supervision, Project administration, Funding acquisition, Conceptualization, Writing – review & editing.

Declaration of competing interest

The authors declare that they have no known competing financial interests or personal relationships that could have appeared to influence the work reported in this paper.

Appendix A. Supplementary data

Supplementary data to this article can be found online at https://doi.org/10.1016/j.atmosenv.2021.118371.

on background days (0.71 ± 0.14), owing in part to a strong presence of sea salt and reduced presence of more hydrophobic species such as those of a carbonaceous or mineral-dust nature. Finally, periods of heavy rainfall were shown to effectively decrease both $CCN_{0.2\%}$ and $CCN_{1.0\%}$ concentrations. However, the rate varied at which such concentrations increased after the rain. This work contributes knowledge on the nucleating ability of African dust and BB in a marine environment after varying periods of atmospheric transport (days to weeks). The results can be used to understand the hygroscopicity of these air mass types, predict how they may influence cloud properties, and provide a valuable model constraint when predicting CCN concentrations in comparable situations.

Keywords

CCN; African dust; Smoke; Aerosol-cloud interactions; ACTIVATE; EVS-3

1. Introduction

The largest uncertainty in the anthropogenic contribution to climate change is the radiative forcing due to aerosol-cloud interactions (IPCC, 2013). Accurately quantifying concentrations of cloud condensation nuclei (CCN) is an integral part in reducing this uncertainty due to their role in determining cloud radiative properties and longevity (Albrecht, 1989; Rosenfeld et al., 2008; Twomey, 1974). Closure studies, in which in situ CCN concentrations are compared to those calculated based on measured input data (e.g., composition, size distribution), have been successful under background aerosol conditions (Chuang et al., 2000; Dusek et al., 2003; Gasparini et al., 2006; Rissler et al., 2004; Stroud et al., 2007; Vanreken, 2003). Urban environments present a greater challenge due to the increased complexity in the size and composition of the aerosols present (Crosbie et al., 2015; Cubison et al., 2008; Sotiropoulou et al., 2007). Sotiropoulou et al. (2007) reports that CCN model predictions in places impacted by urban pollution and biomass burning are most uncertain. With over half of the world's population living in urban environments, a number that is only growing (United Nations, 2018), there is increasing urgency to reduce error in model-predicted CCN concentrations in such settings to better forecast cloud properties, climate change, weather, and surface air quality (Andreae and Rosenfeld, 2008; Cubison et al., 2008; Molina et al., 2007).

Populated coastal areas create an environment in which anthropogenic and natural aerosols converge, but the resulting air masses and their properties remain unclear (Cruz et al., 2019; Cubison et al., 2008; Sotiropoulou et al., 2007). Kummu et al. (2016) reports that 39% of the global population in 2010 lived within 100 km of a coastline and that this number will continue to increase until at least 2050. With sea salt and dust comprising the majority of global aerosols by mass, the merging of these natural aerosol types and human-generated particles is inevitable (Huneeus et al., 2011; Middleton and Goudie, 2001).

Virginia Key, an island just east of Miami, Florida, provides an excellent location to study CCN since it hosts a complex mixture of aerosols, originating locally, regionally, and from distant continents. The resulting mixture of aerosols is ideal for challenging and improving

models (Klejnowski et al., 2013). Virginia Key experiences periodic influence from Miami's urban emissions, such as those from shipping activity (Hu et al., 2021) and fossil fuel combustion (Klejnowski et al., 2013). Additionally, the island is subject to the constant presence of marine aerosol types (e.g., sea salt, organic matter, and those derived from dimethyl sulfide [DMS]; Quinn and Bates, 2014) characteristic of coastal areas (Gantt et al., 2015; Nolte et al., 2015). Of particular relevance to this location are episodic intrusions of transported African dust, which have been the subject of numerous past works (Aldhaif et al., 2020 and references therein; Prospero, 1999; Zuidema et al., 2019). African dust reaches southeast Florida year-round but peaks between June and August (Aldhaif et al., 2020; Prospero, 1999; Zuidema et al., 2019), typically including 5–8 episodes each summer (Kramer et al., 2020a). Studies have quantified the arriving mass concentration of African dust (Zuidema et al., 2019), investigated its influence on human health (Prospero et al., 2014) and air quality (Prospero, 1999), and characterized its size distribution (Kramer et al., 2020b; Li-Jones and Prospero, 1998) and chemical properties (Zamora et al., 2011, 2013). However, the influence of African dust on CCN concentrations in southern Florida has received scarce attention, and it is unknown if the dust perturbs CCN concentrations in the area. Many models (e.g., ECHAM5-HAM [Hoose et al., 2008], GLOMAP-bin [Manktelow et al., 2010], EMAC [Pringle et al., 2010], and Meso-NH [Bègue at al., 2015]) consider dust particles as efficient CCN, particularly if they acquire soluble material via internal mixing with other hydrophilic species (Karydis et al., 2011). To our knowledge, the hygroscopic properties of African dust reaching the southeastern U.S. have not been reported in the literature, which adds a degree of uncertainty to how CCN models currently parameterize dust plumes arriving to this region. Weinzierl et al. (2017) shows that CCN concentrations are elevated above background levels during summertime episodes of Saharan dust observed at Barbados, an island 2570 km southeast of Virginia Key. However, both the amount of African dust reaching Virginia Key is consistently less than that arriving in Barbados (Zuidema et al., 2019) and Virginia Key is periodically affected by a more complex, urban mixture of aerosols. Additionally, Denjean et al. (2015) and Kandler et al. (2018) each find the hygroscopicity of supermicrometer African dust particles to not change significantly as they are transported across the Atlantic Ocean to the Caribbean, further motivating interest in how African dust plumes affect the CCN budget of the southeastern U.S.

An additional complexity for the southern Florida coastal area is that it is a receptor site of BB emissions from different source regions. Jaffe et al. (2020) finds Florida to be the fourth highest state in the U.S. for annual area burned in prescribed fires, which occur most frequently in the boreal spring (March–May). One source responsible for these prescribed fires is the largest area for sugarcane production in the U.S., located ~130 km to the northwest of Virginia Key. Between mid-fall and spring (October–May), 50–80% of the plants' foliage is burned before harvesting (Le Blond et al., 2017; Ma et al., 2014) and the resulting BB emissions have been shown to travel to eastern Florida where Virginia Key is located (Sevimoğlu and Rogge, 2015, 2016, 2019). Additionally, BB emissions from deforestation and crop residue fires in Central America (Wang and Christopher, 2006; Wang et al., 2006), Mexico (Kreidenweis et al., 2001), the Yucatan peninsula (Yokelson et al., 2009), Cuba (Brey et al., 2018), and the southeastern U.S. (Roy et al., 2018) have also been shown to reach Florida. Many studies have looked at the nucleating ability of BB aerosol

particles (e.g., Bougiatioti et al., 2016; Hennigan et al., 2012; Lee et al., 2010; Pöhlker et al., 2018) and found CCN concentrations generally increase amid BB plumes. However, the exact effect of BB on CCN concentrations is dependent on the fuel source (Chen et al., 2019), background aerosol properties (Pöhlker et al., 2018), and aging of the emissions (Bougiatioti et al., 2016; Hennigan et al., 2012). Each of these conditions differs between Virginia Key and the locations investigated in previous studies, so it is not yet known how the different sources of fire mentioned above influence CCN concentrations in this region. Liu et al. (2013) predicts that the southeastern U. S. will experience a longer fire season in the future, and thus, understanding the effects of BB on CCN in this area is critical.

Another benefit of investigating CCN concentrations in southeast Florida is that aside from the complexity of aerosol sources, there is a wide range of meteorological conditions that both impact aerosol characteristics and are, in turn, potentially influenced by CCN themselves. In particular, Virginia Key experiences greater rainfall than most of the U.S. (Smith et al., 2019), and this precipitation peaks just before the influence of African dust is highest (Abiy et al., 2019; Zuidema et al., 2019). Many particles, including CCN, can be removed during rain episodes (Ohata et al., 2016). In order to improve climate models, not only does the nucleating ability of aerosols need to be understood, but the removal of CCN through wet scavenging needs to be as well.

The effect of episodic Saharan dust and BB emissions superimposed on background aerosol conditions, as well as the implications of wet scavenging, on CCN concentrations in this region is unknown but essential to study in order to improve models simulating aerosol particles, clouds, and precipitation. In response to this knowledge gap, this study aims to characterize the behavior of CCN concentrations in southeast Florida and to identify how they are impacted by the influence of different aerosol types and rain conditions. This work specifically examines in situ data for CCN concentrations measured at different supersaturations (SSs) on Virginia Key and uses complementary datasets to address the relative importance of dust, smoke, and rainfall on CCN properties.

2. Experimental methods

This study relies on a variety of datasets that are summarized in Table 1. A brief description of each dataset is provided below. Furthermore, while some data were collected at sites adjacent to Virginia Key, the results in Section 3 still refer to Virginia Key for simplicity of discussion.

2.1. CCN concentrations

A single chamber CCN counter from Droplet Measurement Technologies (DMT; Roberts and Nenes, 2005) measured CCN concentrations at SSs of 0.2 and 1.0% at south Florida's Cloud-Aerosol-Rain Observatory (CAROb; http://carob.rsmas.miami.edu) at the Rosenstiel School of Marine and Atmospheric Science (25.75° N, 80.25° W), located on Virginia Key, approximately 4 km east of Miami. Information on how the instrument was calibrated can be found in the supplemental document (Section S1). Ambient sampling was conducted from March to September 2013, July to September 2017, and April to June 2018 for 5 min at each SS during the listed months of 2013 and for 10 min at each SS during the listed months in

2017 and 2018. To ensure the instrument column had been given sufficient time to stabilize at the new SS, the first 2 min (for the 2013 dataset) and 4 min (for the 2017 and 2018 datasets) of CCN data were removed for each measurement period at a given SS. After all data for the three years were combined, the CCN concentrations were sorted by SS. CCN concentrations falling three standard deviations above the mean were removed from the dataset (Anscombe, 1960; Miller, 1991) for each SS group (i.e., 0.2% SS and 1.0% SS). The instrument continuously sampled ambient aerosol particles unless impeded by weather events, such as hurricanes.

2.2. Dust mass concentrations

To quantify African dust loadings, daily bulk aerosol samples were collected from a 16-m-fold-over tower on the roof of a 12-m building at the CAROb facility. Hi-Vol sampling pumps pulled air through 20 cm × 25 cm Whatman-41 filters (W-41) at a flow rate of ~1 m^3 min^{-1}. The W-41 filters have a dust collection efficiency of 95% or better (Kitto and Anderson, 1988). In order to minimize contribution of local sources, sampling only occurred when the winds came from the east (45°–202°) at speeds greater than 1 m s^{-1}. The assumption is that under such collection criteria, the measured dust had a high likelihood of originating from North Africa and local sources were minimized. Aerosol samples collected using the described methods were only considered in the final dataset if sampling exceeded 10% of the available period (e.g., 2.4 h for a full day). The W-41 filters were rinsed in triplicate then put in a 500 °C furnace for 14 h and the ash residue was weighed, corrected by a factor of 1.3, and assumed to be mineral dust, resulting in a standard error of ±0.1 μg m^{-3} for concentrations below 1 μg m^{-3} and 10% for higher concentrations. More details regarding the sampling, processing, and conversion of dust mass on filters into dust mass concentration can be found in Zuidema et al. (2019) and Prospero (1999).

Sample collection for African dust typically occurred daily from May to September, and twice weekly for all other months. In this study, the dust mass concentration listed for a given sampling period was attributed to the day on which the filter was collected. This was a potential source of error when measurement periods spanned several days. Finally, a lightning strike hit the tower in May 2013, and the tower was not replaced until late July 2013, which means data are unavailable for this period.

2.3. Micropulse lidar

Images from a Sigma Space micropulse lidar (MPL) with polarization (MPL-P, model MPL-4B-IDS-532; Delgadillo et al., 2018) were used to confirm the most significant episodes of dust. This instrument is also part of the CAROb facility. The MPL transmitted a 532 nm beam of light alternating between co-polarized and cross-polarized states and measured the polarization of the returning signal.

2.4. IMPROVE

In order to quantify concentrations of aerosol types other than dust (Section 2.2) present at Virginia Key and their relationship to CCN concentrations, data were used from a monitoring site in south Florida (Everglades NP [EVER1]: 25.39° N, 80.68° W, elevation = 1 m above sea level) associated with the Interagency Monitoring of Protected Visual

Environments (IMPROVE) network. The site is located ~65 km southwest of the CARObstation. Details on the collection, quality control, and conversion to air mass concentration can be found elsewhere (Chow et al., 2015; Hand et al., 2012). IMPROVE data were used to characterize days with the most and least influence from smoke by examining concentrations of organic carbon (OC) and elemental carbon (EC) in particulate matter (PM) with aerodynamic diameters less than or equal to 2.5 μm ($PM_{2.5}$). Schlosser et al. (2017) found OC and EC to be some of the most enhanced species during wildfires based on IMPROVE data, so they are used in this study to mark the signature of smoke. Additionally, the monthly profiles of major components contributing to $PM_{2.5}$ are shown (sea salt, fine soil [FS], ammonium nitrate [AmmNit], ammonium sulfate [AmmSul], OC, and EC), based on the method of Hand et al. (2019). Lastly, concentrations of PM_{coarse} are also reported, representing the difference between PM_{10} and $PM_{2.5}$.

2.5. NADP/NTN

Wet deposition composition data were obtained from the Everglades National Park-Research Center (25.39° N, 80.68° W, elevation = 2 m above sea level) site affiliated with the National Atmospheric Deposition Program National Trends Network (NADP/NTN). Information regarding the analysis and quality assurance of NADP data can be found in Gartman (2017). Weekly concentration data were attained for eight water-soluble ions (Ca^{2+}, Mg^{2+}, K^+, Na^+, NH_4^+, NO_3^-, Cl^-, SO_4^{2-}). For this study, data were specifically used from the summer (June–August) of 2017. All reported concentrations were weighted by the volume of precipitation collected in a particular week relative to the total volume collected from June–August 2017. Average relative mass fractions were then determined from the volume-weighted concentrations.

2.6. PERSIANN rain data

Daily and hourly rain data were obtained from the Center for Hydrometeorology and Remote Sensing (CHRS) Precipitation Estimation from Remotely Sensed Information using Artificial Neural Networks (PERSIANN) system. Data were obtained for the same location as the CARObinstrument suite. PERSIANN rainfall is generated from geostationary longwave infrared imagery and adaptive training of the neural network from independent rainfall measurements. Further information on the algorithms and data used is available in Nguyen et al. (2019).

2.7. MesoWest meteorological data

Observations of temperature, relative humidity (RH), near-surface wind speed, and near-surface wind direction were obtained at 5-min temporal resolution from MesoWest, a network of surface stations distributed across the U.S. (Horel et al., 2002). Data provided through MesoWest come from various participating organizations including government agencies, private firms, and educational institutions around the country. As described in Horel et al. (2002), quality control procedures are performed on all observations, and a quality control flag is assigned to each dataset before it becomes publicly available. For this study, observations were used from the KMIA station at the Miami International Airport

(25.79° N, 80.32° W, elevation = 3 m above sea level, 15 km northwest of CARObb) assigned with the highest quality flag (“OK”).

2.8. Model and reanalysis datasets

To aid in air mass source identification for smoke and African dust, back trajectories of 100 and 300 h were obtained from the Hybrid Single-Particle Lagrangian Integrated Trajectory (HYSPLIT) model (Rolph et al., 2017; Stein et al., 2015) at ending altitudes of 200, 1000, and 2000 m above ground level at CARObb (25.75° N, 80.25° W). The trajectory time selected depended on the proximity of the source. For example, 300 h were necessary to trace dust back to Africa, whereas only 100 h were needed when the smoke originated over the southeastern U. S. Trajectories were created with 3-h resolution using the National Centers for Environmental Prediction/National Center for Atmospheric Research (NCEP/NCAR) reanalysis data with the “model vertical motion” method. To further confirm HYSPLIT results, *earth* (earth.nullschool.net), a global animation of wind, weather, oceanic, and aerosol-related conditions, was used to view wind trajectories and speeds present at CARObb (at the surface) and at 850, 700, and 500 hPa during smoke and African dust events. *Earth* wind data and imagery come from the National Weather Service (NWS), NCEP, the National Oceanic Atmospheric Administration (NOAA), and the Environmental Modeling Center (EMC), and are available at 3-h resolution.

The Navy Aerosol Analysis and Prediction System (NAAPS) was used to verify the presence of African dust, smoke, and background conditions for specific days occurring during the study period. The selection of such days is discussed in the following section. NAAPS images from the Aerosol Modeling archive for the Caribbean were created using global meteorological fields from the Navy Global Environmental Model (NAVGEM; Hogan and Rosmond, 1991) and have been successfully used in other studies to verify the transport of dust (Cottle et al., 2013; Lopez et al., 2015; McKendry et al., 2007; Wells et al., 2007; Wu et al., 2015) and smoke (Dementeva and Balzhanov, 2018; Ge et al., 2017; Khan et al., 2019; Markowicz et al., 2017; Xian et al., 2013). Plots generated by the NAAPS model display the surface concentration of smoke and dust in units of μg m^{-3} at a 6-h resolution over a 4-day period.

Reanalysis data from the Modern-Era Retrospective Analysis for Research and Applications, Version 2 (MERRA-2) model were used to confirm the source of smoke and African dust on specific days at Virginia Key. Hourly resolved images for “OCCMASS” and “DUCMASS25” from the M2T1NXAER (hourly, time-averaged, single-level assimilation aerosol diagnostics V5.12.4) product revealed the OC column mass density and $PM_{2.5}$ dust column mass density, respectively. Just as OC was mentioned to be a tracer of smoke in Section 2.4, MERRA-2’s OC product was used to visualize the transport of smoke to Virginia Key. The images generated from MERRA-2 reanalysis data for days leading up to and during each smoke or dust event were viewed in series for easier identification of the source and to observe air mass transport behavior at Virginia Key. Additionally, MERRA-2’s M2T1NXFLX (hourly, time-averaged, single-level assimilation surface flux diagnostics V5.12.4) product provided planetary boundary layer heights (PBLHs) at a spatial resolution of 0.5 ° × 0.625 ° and hourly temporal resolution (Davy, 2018; Molod et al., 2019).

2.9. Air mass type criteria

To understand the influence of smoke and African dust on CCN concentrations at Virginia Key, days with the most influence from these aerosol types were selected using the criteria shown in Table 2. For simplicity, days influenced the most by African dust and smoke are hereafter referred to as “dust days” and “smoke days”, respectively. To contrast with dust and smoke days, background days were identified as days that had minimal influence from smoke, African dust, and rain. These days were intended to serve as a control group to reflect CCN concentrations at Virginia Key under minimal influence from African dust and BB emissions. The amount of rain observed on background days was restricted to low values (<4 mm) to eliminate the possibility that CCN concentrations on background days deviated from that on smoke or dust days due to wet scavenging via especially high levels of rainfall (Ohata et al., 2016), and not just because of the absence of dust or smoke. Although many sources were available to determine the presence of dust and smoke, priority was given to in situ measurements: IMPROVE data for smoke and the W-41 filter concentrations collected at CARObfor African dust. Aerosol fields obtained from NAAPS and MERRA-2 were additionally used to confirm the presence of smoke and dust on smoke and dust days, respectively, as well as the absence of such aerosols on background days. Percentiles shown in Table 2 are based on data for days only when CCN measurements were also available. Lastly, all other sampling days that did not qualify as being smoke, dust, or background days were simply collected into a final category called “other” days.

2.10. Data organization and analysis method

Concentrations of CCN at 0.2 and 1.0% SS ($CCN_{0.2\%}$ and $CCN_{1.0\%}$, respectively) were extracted for each day listed in Table 2 and grouped together by category. The MATrix LABoratory (MATLAB) computer program’s “anova1” and “multcompare” functions were used to determine if statistically significant differences in $CCN_{0.2\%}$ were present between any of the four categories (smoke, dust, background, and “other”). The “anova1” function assumes all sample populations are normally distributed. Winer et al. (1991) report that analysis of variance (ANOVA) tests are still applicable when data are not normally distributed as long as sample populations are reasonably large and similar in size. Blanca et al. (2017) show that ANOVA tests are robust for non-normally distributed sample populations with as little as 30 points. Since there were at least 9000 CCN measurements at each SS for each air mass category in this study, we assume ANOVA tests were an appropriate means to determine statistically significant differences between categories. If these tests returned a p value lower than 0.05 when comparing $CCN_{0.2\%}$ between two categories, the categories were considered to have statistically significant different means at a 95% confidence level. This analysis was repeated for $CCN_{1.0\%}$. The one Hz CCN data were then averaged on an hourly basis and the ratio of $CCN_{0.2\%}$:$CCN_{1.0\%}$ was determined for each hour. More information on the methods used in this procedure can be found in Section S2. MATLAB’s “anova1” and “multcompare” functions were again utilized to determine if differences in ratios observed for the various categories were statistically significant. A higher average ratio for a certain category implies the CCN (i) are shifted to larger particle sizes that can more easily activate and/or (ii) are more hygroscopic in terms of their chemical composition.

Finally, the one Hz $CCN_{0.2\%}$ and $CCN_{1.0\%}$ and the hourly ratios were analyzed on an hourly basis for each category. This was done to extract any diurnal trends that could not be captured in the lumped statistical tests described above. To show deviations from the entire dataset, the diurnal trend for all sampling days were presented alongside the results for each category.

3. Results and discussion

3.1. Aerosol profile

3.1.1. Annual composition climatology—To provide context for the CCN data, monthly-averaged aerosol and rain characteristics are first summarized from the IMPROVE and PERSIANN datasets, respectively, for the years relevant to this study (2013, 2017, and 2018). In general, Virginia Key is affected by biomass burning from the Americas in the spring and African dust in the summer, with anthropogenic pollution and sea-spray aerosols affecting the site year-round. Monthly trends in the six components of Virginia Key's $PM_{2.5}$ (FS, sea salt, OC, EC, AmmSul, and AmmNit) reflect the known timing of these air masses (Fig. 1). FS increases between June and August (monthly mean range: 1.61–2.57 μg m^{-3}) compared to the rest of the year (0.11–1.18 μg m^{-3}), which aligns with the months experiencing the strongest influence from African dust (Zuidema et al., 2019). Li-Jones and Prospero (1998) found one-third to one-half of the African dust aerosols arriving to the southeastern U.S. have diameters smaller than 2.5 μm, which is the size range examined for FS in Fig. 1. An important note is that the aerosol sampling at the IMPROVE site is not restricted to certain conditions like the dust sampling at CARObe. Therefore, FS captured at the IMPROVE site can originate from places besides Africa, such as the continental U.S. (Aldhaif et al., 2020; Brandli et al., 1977). OC and EC are collectively highest between January and April (0.80–1.33 μg m^{-3} for OC and 0.17–0.30 μg m^{-3} for EC) as compared to the rest of the year (0.40–0.65 μg m^{-3} for OC and 0.05–0.16 μg m^{-3} for EC). The higher OC and EC levels, especially in March, are temporally coincident with the peak of the prescribed burning season in the southeastern U.S. (Jaffe et al., 2020; McCarty et al., 2007), and also biomass burning in Central America (Wang et al., 2006a, 2006b), Cuba (Brey et al., 2018), Mexico (Kreidenweis et al., 2001), and the Yucatan peninsula (Yokelson et al., 2009). Aside from the elevated levels in the spring, Virginia Key has a consistent presence of OC and EC year-round due to persistent sources such as living organisms (Szidat et al., 2009), automobile exhaust, and other forms of fossil fuel combustion (Qi et al., 2018). Sea salt particles are emitted as waves break year-round on nearby coastlines, which is reflected in the presence of sea salt in each month (0.38–0.90 μg m^{-3}). Prospero (1999) actually showed sea salt concentrations on Virginia Key are slightly higher in the spring owing to stronger winds, which agrees with our results for higher values in April and May. AmmSul and AmmNit are relatively stable in mass concentration throughout the year (1.24–2.13 μg m^{-3} and 0.32–0.59 μg m^{-3}, respectively) owing to consistent precursor emissions (e.g., SO_2, NO_x, NH_3) from various nearby sources such as combustion, shipping, and agriculture (Bouwman et al., 1997; Schulze et al., 2018). Sulfate is additionally formed from oceanic DMS emissions (Barnes et al., 2006; Charlson et al., 1987; Keller, 1989).

Similar to total $PM_{2.5}$, PM_{coarse} is generally highest between March and August (7.57–19.16 μg m^{-3}) excluding May (6.30 μg m^{-3}), compared to the rest of the year (5.23–6.40 μg m^{-3}; Fig. 1). The stark maximum in March was both a persistent feature for all three years included in this study and consistent with the biomass burning season both in the region and in more distant regions such as Mexico, Central America, and Cuba. Coarse soil particles can efficiently be entrained in burning plumes owing to the turbulence and buoyancy by flames and burn fronts (Clements et al., 2008; Gaudichet et al., 1995; Kavouras et al., 2012; Maudlin et al., 2015; Palmer, 1981; Popovicheva et al., 2014; Sturtz et al., 2014). Schlosser et al. (2017) found that mass concentrations of fine soil and PM_{coarse} can persist, and even be higher, at sites downwind from sources of BB; this finding is relevant to this study as many of the sources of smoke mentioned above are at a considerable distance from Virginia Key. Additionally, southeastern Florida experiences reduced rainfall from November to March (Abiy et al., 2019). Decreased precipitation over this time period may lead to a lower soil moisture content by March. Wind speeds increase from winter to spring in southeast Florida (David et al., 2019), which, in tandem with lower soil moisture, may increase local dust emissions that contribute to the PM_{coarse} peak in March. The second PM_{coarse} peak in July can plausibly be linked to the increased presence of African dust, which is presumably much less than the March PM_{coarse} peak owing to the greater transport distance from Africa that would result in the largest particles being removed (Aldhaif et al., 2020; Kramer et al., 2020b; Prospero, 1999). There is more variability in PM_{coarse} throughout the year on Virginia Key as compared to $PM_{2.5}$, which may be due to episodic events enriched with dust particles contributing more to PM_{coarse} than $PM_{2.5}$.

3.1.2. Annual african dust trends—African dust concentrations collected at CAROb during each month of 2013, 2017, and 2018 (Fig. 2) reflect the FS trend observed in Fig. 1 and long-term African dust behavior observed at Virginia Key (Prospero, 1999; Zuidema et al., 2019). Variability is low and outliers are nearly nonexistent in the late fall, winter, and early spring. However, between May and September, the size of the quartiles and the number of outliers both increase coincident with when the bulk of the African dust arrives at southeastern Florida (Zuidema et al., 2019). To reinforce the episodic nature of African dust events (Kramer et al., 2020a), dust levels can suddenly spike above 30 μg m^{-3} when a strong African dust episode arrives. This is in contrast to most days, including those in the summer, where dust levels are typically less than 5 μg m^{-3}.

In situ and remote sensing observations at the CAROb site allow for a deeper examination of major dust events occurring during the three-year study period. Since dust particles have depolarization ratios exceeding most other aerosol types in the study region (Groβ et al., 2013; Haarig et al., 2017), MPL data reveal periods with heavy dust influence (Fig. 3; see also Kramer et al., 2020b for more discussion). Four dust days, in particular, during the summer and early fall of 2017 demonstrate the episodic nature of African dust events. More specifically, low depolarization ratios (<0.13) were observed above 1.5 km altitude for a few consecutive days followed by sharp increases (up to ~0.20) coinciding with dust events that typically lasted 3–5 days. The altitude to which the depolarization ratio was enhanced was related to the severity of the dust event. For example, the highest African dust mass concentration measured during the study (73.32 μg m^{-3}) on August 4, 2017 coincided with

elevated depolarization ratios (~0.20) up to ~3 km. In contrast, the weakest of the four dust days (33.42 μg m^{-3}) on July 26, 2017 exhibited enhanced ratios (~0.20) up to only ~1.5 km. The heights to which depolarization ratios were affected by African dust are consistent with typical observed dust plume heights of 1.5–3 km in the Saharan Air Layer (SAL) over Barbados (Haarig et al., 2019), and at times reach above 4 km (Kramer et al., 2020b).

Dust mass concentrations and CCN concentrations in this study are based on surface measurements, but Fig. 3 shows dust is also present in the planetary boundary layer (PBL) and above. This implies the relationship between CCN and dust mass concentrations analyzed at the surface in this study may also be applicable at altitudes relevant to cloud formation. The rapid reductions in dust concentrations after the significant bursts (Fig. 3) can potentially be linked to factors such as winds removing the plumes from the area in addition to precipitation scavenging, both of which have been shown to decrease aerosol concentrations in other locations (Cugerone et al., 2018; Luan et al., 2019; Ohata et al., 2016). As shown in the next section, Virginia Key experiences intense rainfall in the summer months when African dust is at its peak, and thus the influence of precipitation on CCN removal is of interest to study.

3.2. Precipitation profile

Precipitation data for Virginia Key from the three years relevant to this study reveal a wide range in rain rates (Fig. 4a). Although the most common rain rates observed are between 0 and 3 mm day^{-1}, rates as high as 76.5 mm day^{-1} also occurred during the study period. Fig. 4b shows the wide range of rainfall received during an annual cycle. Virginia Key experiences intense rainfall starting in May and lasting until September. The range of average monthly rainfall observed in this rainy season is from 69.66 ± 25.49 mm (August) to 134.97 ± 77.61 mm (June). The lowest rain amounts are during the winter, ranging from 4.32 ± 2.99 mm (February) to 7.50 ± 2.41 mm (December). The much larger standard deviations for the months with the most rain point to the episodic nature of rain events, motivating interest in how such events scavenge CCN in the region. While the monthly mean data for $PM_{2.5}$ and PM_{coarse} do not show a significant reduction between May and September, the speciated $PM_{2.5}$ results in Fig. 1 show that most constituents other than fine soil are reduced in concentration between those months owing presumably in some part to enhanced wet scavenging.

3.3. Characteristics of air mass types

The wide range of months covered in this study allowed for both (i) a sufficiently large dataset to obtain reliable statistics regarding the amounts of African dust, OC, EC, and rainfall impacting Virginia Key, and (ii) an opportunity to study the sensitivity of CCN concentrations to high loadings of seasonally-dependent aerosol types, such as African dust and particles from BB. This section focuses on the former while Section 3.4 pertains to the latter.

Over the three-year study period, CCN data were obtained for 315 days. Thirteen days were classified as either dust, smoke, or background days (see Section 2.9 and Table 2). The remaining 302 days were categorized as “other” days. Since the “other” category accounted

for 96% of the sampling days, it can be considered to best represent typical conditions at Virginia Key during the late spring to early fall (i.e., days experiencing moderate levels of African dust and/or BB aerosols). The major characteristics of each category are as follows and summarized in Table 3:

- Background days had relatively low concentrations of African dust, OC, and EC compared to other categories. NAAPS data confirmed a low presence of dust and smoke at the surface for each background day, with examples shown in Fig. 5a–b.
- The average African dust mass concentration on dust days was more than two orders of magnitude greater than that of background days. For example, the dust surface concentration on the August 04, 2017 dust day (73.32 μg m^{-3}; Fig. 5c) was noticeably higher than that on the background day (Fig. 5a). None of the five smoke days experienced African dust, which is not surprising since all smoke days occurred in months (March and April) preceding the main African dust period (Fig. 2).
- The timing of smoke days coincided with the peak season (March–May) for regional prescribed fires. Smoke enhancements in and around Virginia Key are evident when comparing Fig. 5d and b. The average concentrations of OC and EC on smoke days were at least an order of magnitude higher than those on background days. Additionally, PM_{coarse} was noticeably higher on smoke days, presumably because of the proclivity for coarse particles to become entrained in flames and burn fronts, as mentioned in Section 3.1.1.
- "Other" days had modest influence from African dust, OC, and EC, but with concentrations of these species still considerably higher than those on background days. Although low rain rate averages were present for each category, the "other" category exhibited the highest mean and exhibited the most variability (3.45 ± 6.96 mm day^{-1}). This is likely due to the "other" category encompassing far more days of data where heavier precipitation is inevitable for an area such as southern Florida that can have extensive rainfall, especially in the summer (Fig. 4).

3.4. CCN behavior

3.4.1. Air mass type comparisons—Average and standard deviations of CCN concentrations for the four air type categories are compared here (Table 3). All categories were found to have statistically significantly different means in $CCN_{0.2\%}$ at a 95% confidence level (p value < 0.05). The category with the lowest average $CCN_{0.2\%}$ was dust (289 ± 104 cm^{-3}), followed by "other" (343 ± 279 cm^{-3}), background (373 ± 279 cm^{-3}), and smoke (1405 ± 976 cm^{-3}). The ANOVA test performed on the $CCN_{1.0\%}$ yielded p values below 0.05 when comparing all categories except between dust and background categories. In ascending order, average $CCN_{1.0\%}$ were as follows: background (584 ± 323 cm^{-3}), dust (591 ± 302 cm^{-3}), "other" (753 ± 564 cm^{-3}), and smoke (3337 ± 1252 cm^{-3}). These results reveal multiple important findings discussed subsequently.

First, CCN on dust days were not clearly elevated above those on background days, despite the substantial difference in African dust concentrations for the two categories. This may be due to African dust plumes being comprised of larger particles with lower number concentrations, as will be discussed in Section 3.5.1. The second notable result is how much higher CCN were on smoke days than for any of the other categories, a result that has been observed at multiple other locations (e. g., Bougiatioti et al., 2016; Kacarab et al., 2020; Pöhlker et al., 2018; Zheng et al., 2020). Despite high PM_{coarse} concentrations on smoke days (Table 3), it is unlikely these larger particles contributed significantly to the elevated CCN concentrations. A rough calculation assuming all PM_{coarse} aerosols were dust (density of 2.6 g cm^{-3}; Rocha-Lima et al., 2018) with a diameter of 2.5 μm (10 μm), suggests the number concentration for these aerosols would be as low as 2.09 cm^{-3} (0.03 cm^{-3}). Thus, it is more likely the increase in smaller particles, evident in the increased mass concentrations of $PM_{2.5}$ species such as OC, EC, AmmNit, and AmmSul on smoke days (Table 3), induced the higher CCN concentrations. Third, background days had the second highest average $CCN_{0.2\%}$ concentration and nearly the lowest average $CCN_{1.0\%}$ concentration. To reconcile the difference, it is presumed that background aerosols are composed of larger and/or more water-soluble particles that were fewer in total number as compared to other categories. The lowest mass fractions of relatively hydrophobic species (i.e., OC and EC; Li et al., 2016) were observed on background days in addition to the highest mass fraction for sea salt, a well-known large and hygroscopic aerosol type (e.g., Clarke et al., 2003; Petters and Kreidenweis, 2007; Schlosser et al., 2020, Table 3). The combined effect of reduced non-hygroscopic particles with increased sea salt influence may explain the higher (lower) concentrations of $CCN_{0.2\%}$ ($CCN_{1.0\%}$).

To gain additional insight into the relative hygroscopicity associated with each category, average ratios between $CCN_{0.2\%}$ and $CCN_{1.0\%}$ are next discussed. The ANOVA test performed on the ratios only returned p values below 0.05 when comparing the background category to all others. The average ratio for the background category (0.71 ± 0.14) was ~30% higher than that of other categories, which had similar ratios amongst themselves (dust: 0.54 ± 0.17; smoke: 0.55 ± 0.17; “other”: 0.55 ± 0.21). As mentioned, background days had some of the highest mass fractions for hygroscopic constituents, such as sea salt (0.17 ± 0.04) and AmmSul (0.31 ± 0.14), in combination with the lowest mass fractions for more hydrophobic species such as OC (0.04 ± 0.01) and EC (0.00 ± 0.00). Thus, a higher fraction of the total CCN may have been able to activate at the lowest SS, resulting in a higher average ratio.

The fact that the average ratio for the smoke category does not deviate from the dust and “other” categories is an intriguing result, especially considering the enormous discrepancy in the actual CCN concentrations between the categories. Furthermore, aerosol chemical composition appears to be different between these three categories (Table 3). While coincident aerosol measurements of composition and size distribution are not available for smoke air masses, the results suggest that the combined influence of the two aerosol properties yields nearly identical $CCN_{0.2\%}$:$CCN_{1.0\%}$ ratios as two other air mass types (dust and “other”) stemming from very different sources. As will be shown subsequently, both the smoke and African dust air masses were subject to transport times on the order of days.

Thus, it is possible the two underwent comparable aging processes, resulting in similarly hygroscopic properties.

3.4.2. Diurnal trends—Diurnal patterns provide insight into possible relationships between median $CCN_{0.2\%}$ and $CCN_{1.0\%}$ concentrations and the PBLH, periods of peak human activity, oxidation of hydrophobic aerosols, land-sea breeze circulation (Delgadillo et al., 2018), and particle growth mechanisms (e. g., condensational growth, coagulation) over the course of a day. Median $CCN_{0.2\%}$ concentrations (Fig. 6a) decrease gradually after midnight. As will be shown in the case studies (Section 3.5), these early morning hours are marked by increases in PBLH and temperature. From 7:00 to 8:00 there is an increase in $CCN_{0.2\%}$ concentration, possibly owing to increased fresh fossil fuel combustion aerosols from commuter traffic. However, this morning increase is not observed for $CCN_{1.0\%}$ concentrations until 9:00 (Fig. 6b). After the morning rush hour (7:00 to 9:00), concentrations decrease until midafternoon (16:00 [$CCN_{0.2\%}$] and 14:00 [$CCN_{1.0\%}$]), which aligns with observed increasing PBLHs and sea breezes bringing in relatively clean marine air. The subsequent increase in $CCN_{0.2\%}$ and $CCN_{1.0\%}$ at 17:00 and 15:00, respectively, may be related to a combination of afternoon rush hour emissions, secondary aerosol formation associated with higher photo-oxidation potential at this time of day, and growth of fine mode particles as observed in other regions, such as Los Angeles (Hersey et al., 2011; Mei et al., 2013) and near San Diego (Gaston et al., 2018). Following this midafternoon enhancement, $CCN_{0.2\%}$ concentrations remain elevated into the night, whereas $CCN_{1.0\%}$ concentrations fluctuate until midnight. The steadily elevated $CCN_{0.2\%}$ concentrations may be the result of decreasing PBLHs and/or a land breeze coming from the mainland in tandem with the cumulative effects of aerosol oxidation and/or growth via coagulation throughout day. In contrast, $CCN_{1.0\%}$ concentrations are more variable into the evening presumably owing to reductions in sources of fresh emissions and larger particles acting as a coagulation sink for smaller ones, resulting in no change in $CCN_{0.2\%}$ but a reduction in $CCN_{1.0\%}$.

The size of the inner quartiles is greatest from 17:00 to 22:00 for $CCN_{0.2\%}$ and from 12:00 to 17:00 for $CCN_{1.0\%}$. Variability may be greater for $CCN_{0.2\%}$ later in the day due to the multitude of influences relevant at this time (i.e., secondary aerosol formation and aerosol growth; decreasing PBLH; and emissions from evening anthropogenic activity). In contrast, variability may be highest for $CCN_{1.0\%}$ concentrations in the early afternoon when activities producing fresh aerosols, such as those from fossil fuel combustion, are arguably more prevalent.

Categorical $CCN_{0.2\%}$ concentrations (i.e., smoke, dust, background) reveal two main modes, albeit there is noise owing to limiting data volume: one in the morning (5:00 and 8:00 [smoke], 5:00 to 7:00 [dust], and 7:00 and 9:00 [background]), and one in the evening (19:00 to 20:00 [smoke], 21:00 [dust], and 16:00 and 19:00 [background]). Categorical $CCN_{1.0\%}$ concentrations exhibit diurnal trends that are less uniform. Concentrations for smoke and dust categories both climb drastically in the early morning (2:00 to 5:00 [smoke] and 3:00 to 6:00 [dust]), possibly due to a land breeze, whereas background values oscillate. After the steep morning increase, smoke $CCN_{1.0\%}$ concentrations remain relatively elevated for the remainder of the day, whereas those of the dust category fall back down to values observed before the morning peak. Throughout the day, background $CCN_{1.0\%}$

concentrations are relatively variant, but two periods of consistent increase are observed, coincidentally during the morning and afternoon rush hours (5:00 to 8:00 and 16:00 to 19:00).

Diurnal trends for each category differ likely owing to the variability in their sources and transport distance. Diurnal trends in smoke may be governed more by wind patterns and/or the availability of sunlight for photochemical formation on BB aerosol species. Consistent with the previous discussion, it appears the arriving dust plumes may not contribute highly to CCN number concentrations as most of the dust mass is presumably comprised of fewer larger particles. Thus, CCN concentrations on dust days may be dictated by other factors such as local wind patterns and local emissions. Patterns observed for the background category may also depend more on the timing of local activities and meteorology.

The ratio between $CCN_{0.2\%}$ and $CCN_{1.0\%}$ oscillates throughout the day for all categories as well as for the entire dataset (Fig. 6c). The size of the interquartile ranges is relatively constant throughout the day, indicating uniform variability at all hours. The smoke category displays the widest range throughout the day, while the dust category rarely falls outside the second and third quartile of the overall dataset. Ratios between $CCN_{0.2\%}$ and $CCN_{1.0\%}$ may fail to display clear diurnal trends because of the multitude of factors governing the relative amount of $CCN_{0.2\%}$ and $CCN_{1.0\%}$ during a given day.

3.5. Case studies

3.5.1. African dust—Although the study period spanned three years, all four dust days were in 2017, and three of these occurred within a two-week window (Fig. 7). There were days in 2013 and 2018 that also had elevated mass concentrations for African dust (Fig. 2); however, CCN were not available for these particular days so they cannot be considered in this analysis. The highest amount of dust was recorded on August 04, 2017 (73.32 μg m^{-3}), and imagery from MERRA-2 as well as HYSPLIT back trajectories trace its origin to northern Africa (Fig. 8a–b). Although not shown, corresponding images show similar results for the other two dust days shaded in Fig. 7. The dust events indicated in Fig. 7 did more than impact Virginia Key: on these same days, Ramírez-Romero et al. (2021) measured a 300 and 500% increase in $PM_{2.5}$ and PM_{10}, respectively, over the Yucatan peninsula and classified them as “African dust peaks.”

Neither $CCN_{0.2\%}$ nor $CCN_{1.0\%}$ peaked on dust days, but rather on days with a low influence of African dust. The highest CCN concentrations observed in Fig. 7 were on July 30, 2017 and August 02, 2017, days which only received 0.12 and 4.09 μg m^{-3} of African dust, respectively. The $CCN_{0.2\%}$:$CCN_{1.0\%}$ ratio did not exhibit significant variability between dust and non-dust periods. The lack of CCN enhancement on dust days is presumed to be due to high dust mass concentrations not equating to a significant enhancement in number concentration owing to larger and fewer coarse particles. Perry et al. (1997) quantified the sizes of African dust particles reaching east Tennessee during an African dust event and found two main peaks in the mass distribution: one at 0.9 μm and another at ~2.5 μm. Using these diameters as a lower and upper bound, assuming a density of dust of 2.6 g cm^{-3} (Rocha-Lima et al., 2018), and assuming that all dust particles would be CCN-active during an average African dust event for this study (48.17 μg m^{-3} of African dust; Table 3), the dust

would only contribute 49 and 2 cm^{-3}, respectively, to the total CCN budget. These are very low values considering average CCN concentrations at Virginia Key are roughly an order of magnitude higher than this at either SS for all categories.

Therefore, while larger dust particles may be more CCN-active based on their larger size (Kumar et al., 2011), they may not impact the region's CCN budget significantly owing to their low number concentration. Furthermore, assuming the dust particles offer larger surface area than typical background aerosols in the study region, they could act as an efficient coagulation sink for smaller particles resulting in reduced CCN concentrations, but especially at 1.0% SS among where smaller particles activate more easily than 0.2% SS.

The hygroscopicity of the African dust arriving at Virginia Key may also play a role in understanding why CCN concentrations were not elevated above background values. Fresh dust exhibits low hygroscopicity, but its affinity for water can increase if it becomes internally mixed with more hydrophilic species that adhere to the surface of dust particles (Hatch et al., 2008; Levin et al., 1996; Sullivan et al., 2009). This can occur if an African dust plume is confronted with an anthropogenic air mass, where soluble species such as sulfate and nitrate are abundant (Bègue et al., 2015). Additionally, African dust can become more CCN-active following cloud processing (Kumar et al., 2011; Weinzierl et al., 2017). Weinzierl et al. (2017) studied the behavior of an African dust plume over Barbados after it had come in contact with tropical storm Chantal, and found $CCN_{0.2\%}$ concentrations to be significantly higher in the Saharan Air Layer compared to background concentrations at the same altitude. However, if a dust plume is not confronted with a more hygroscopic air mass or does not experience significant cloud processing, it may retain its hydrophobic properties. Denjean et al. (2015) and Kandler et al. (2018) reported instances in which African dust particles arriving to the Caribbean were still externally mixed and had not increased in hygroscopicity.

As we do not know the degree of cloud processing each African dust plume considered in this study experienced in its transit over the Atlantic Ocean, nor if the dust encountered any other air masses, it is difficult to make a statement regarding the dust's hygroscopicity upon reaching Virginia Key. For this reason, there is a stronger case for stating that the observed lack of increase in CCN concentrations with African dust events is due to the low number concentration of these presumably larger particles.

3.5.2. Smoke—A pronounced outcome from this work is how dramatically smoke events increased CCN concentrations at both SSs. Average $CCN_{0.2\%}$ and $CCN_{1.0\%}$ concentrations were 277% and 471% higher, respectively, on smoke days than on background days. Similarly, concentrations were 310% ($CCN_{0.2\%}$) and 343% ($CCN_{1.0\%}$) higher on smoke days than they were on "other" days, despite "other" days having moderate influence from both EC and OC (Table 3). This result implies the BB aerosols transported to Virginia Key in the spring have the most significant influence on CCN concentrations among the air mass types investigated in this study. This is an interesting result considering the observed mass concentrations of EC and OC on smoke days are significantly lower than the dust mass concentrations present on dust days (Table 3); it emphasizes the limitation in using mass concentrations in inferring details about regional CCN budgets that depend more on number

concentrations. Thus, the higher CCN concentrations on smoke days may best be explained in that the transported smoke particles were both more numerous and sufficiently large to be CCN-active as compared to other air mass types.

One of the five smoke days will be discussed in detail in this section: April 20, 2018. Imagery from NAAPS (Fig. 5d) and MERRA-2 (Fig. 8c) show several fires in locations surrounding Virginia Key, such as Mexico, Central America, and the southeastern U.S. on this day. However, both HYSPLIT back trajectories (Fig. 8d) and patterns in the boundary-layer wind direction (Fig. 9b) indicate the BB aerosols impacting Virginia Key on this day were likely from fires to the northwest. Beginning in the evening of April 19, 2018 and extending into the afternoon of April 20, 2018, the wind direction gradually shifted from that of coastal waters (~150°) to that of the fires to the northwest (310°). Coincidentally, CCN concentrations rose during this transition as BB aerosols were presumably transported to Virginia Key (Fig. 9d). In the afternoon on April 20, 2018, the wind direction abruptly changed to that of the open ocean (~100°) and continued to come from this direction for the next few days. This sudden shift in wind direction aligned with a swift decrease in CCN, presumably as (i) clean marine air diluted the existing BB particles in Virginia Key and (ii) prevented additional transport of BB aerosols to Virginia Key. These results highlight how important boundary-layer wind direction is in predicting CCN concentrations at a coastal location such as Virginia Key: winds from the direction of open water can bring in relatively pristine air, but a slight shift in the direction can load the air with continental pollutants in a matter of hours.

Lastly, the $CCN_{0.2\%}$:$CCN_{1.0\%}$ ratio decreased slightly on the smoke day as compared to the other days shown (Fig. 9e). Between 22:00 on April 19, 2018 and 9:30 on April 20, 2018, the ratio dropped from ~0.5 to ~0.3 and remained relatively suppressed until 20:00 on April 20, 2018. At this time, the ratio began increasing back to the values observed before the smoke event as CCN concentrations simultaneously began returning to baseline values. Aerosols on smoke days were characterized by a higher mass fractions of relatively hydrophobic species (i. e., OC and EC; Li et al., 2016) and a noticeably lower mass fraction of sea salt, a hygroscopic aerosol type (Petters and Kreidenweis, 2007, Table 3). This shift in composition may help explain the slightly decreased ratio during the smoke day.

3.5.3. Influence of wet scavenging on CCN concentrations—Fig. 10 is useful for describing how CCN concentrations can change on the order of minutes to hours during and after periods of intense rainfall. Decreases in $CCN_{0.2\%}$ and $CCN_{1.0\%}$ were visible with each rain event, but the rates of decrease and length of the subsequent CCN “recharging” periods varied in each case. The first instance of rain (20:00 on July 30, 2017 to 4:00 on July 31, 2017) was the lightest (Fig. 10f). At first, both $CCN_{0.2\%}$ and $CCN_{1.0\%}$ decreased at similar rates (Fig. 10d), as confirmed by the fairly steady ratio of ~0.55 (Fig. 10e). However, around 21:30, $CCN_{0.2\%}$ plummeted, while $CCN_{1.0\%}$ continued to decrease more gradually. This was reflected in a corresponding dive in the ratio from ~0.55 to ~0.25. Similarly, during the second and third periods of rainfall on July 31, 2017 and Aug 01, 2017, $CCN_{0.2\%}$ also decreased more rapidly than $CCN_{1.0\%}$, as visible in the coincident ratio drops (~0.5 to ~0.32 and ~0.7 to ~0.25 for the second and third rain events, respectively). This finding may imply larger and/or more hygroscopic species were scavenged more efficiently via rainout and/or

washout. In support of this hypothesis, a well-known large and hygroscopic aerosol type, sea salt, was found to be one of the most prevalent species in the precipitation collected by NADP during the months relevant to Fig. 10 (Figure S1). More specifically, Na^+ and Cl^- accounted for 18% and 34%, respectively, of the cumulative volume-weighted ion concentration sum. The volume-weighted average mass ratio of Cl^- to Na^+ was 1.87 ± 0.11, which is markedly close to the reference value for sea water (1.8; Chesselet et al., 1972), suggesting these ions originated predominantly from sea salt.

It appears challenging to predict the length of time necessary for CCN concentrations to "recharge" following a period of rain. For the first rain event shown, CCN concentrations remained relatively low as the rain persisted, then restored to pre-rain levels ~4 h after the rain had stopped. In contrast, it took nearly a day for CCN concentrations to increase even just a small amount after the heaviest period of rainfall (the second event shown). In fact, CCN concentrations were only beginning to recover ~27 h after initially dropping when the third period of rainfall ensued, causing them to rapidly decrease again. Interestingly, during the last rain event, CCN concentrations began to recover even before the rain had stopped, with $CCN_{1.0\%}$ "recharging" at a much faster rate than $CCN_{0.2\%}$. Heavy precipitation may increase the presence of sea spray aerosols due to increased wind, wave breaking, and as falling droplets impact the ocean surface. Varying wind speeds and wind direction may determine if these particles would be detected at CARObor not. Seeing that there are indeterminate fluctuations in $CCN_{0.2\%}$ and $CCN_{1.0\%}$ with different rates and durations of rainfall emphasizes the need to formulate robust CCN-model algorithms that can capture this variability and deliver accurate concentrations in such conditions.

3.6. Comparison of CCN concentrations at Virginia Key to other locations

Results from this study are now compared to those reported at other locations. However, these comparisons are presented with a word of caution as the following studies may have followed different data filtering techniques. Long-range-transport from Africa to the Amazon can bring African dust, African BB aerosol, and marine particles into the Amazon's relatively pristine environment (Barkley et al., 2019; Pöhlker et al., 2018; Prospero et al., 1981, 2014). In the case of such events, $CCN_{0.11\%}$ and $CCN_{1.1\%}$ increased several hundred particles per cubic centimeter above background levels (Pöhlker et al., 2018). In northern Europe, $CCN_{0.63\%}$ increased as much as sevenfold with the arrival of African dust (Bègue et al., 2015). Likewise, $CCN_{0.2\%}$ at 2–4 km altitude near Barbados were five times higher on days with high African dust loadings than on days with low dust loadings (Weinzierl et al., 2017). It is possible CCN concentrations did not increase at Virginia Key due to the increased transport distance from Africa as compared to the aforementioned locations, allowing more opportunity for the dust particles to be removed via gravitational settling or precipitation scavenging.

This study found an increase of 277% and 471% in $CCN_{0.2\%}$ and $CCN_{1.0\%}$, respectively, on days heavily impacted by BB aerosols compared to background conditions. Similar increases have been observed elsewhere. For example, Bougiatioti et al. (2016) found CCN concentrations to increase between 65% and 150% for SSs ranging from 0.2% to 0.7% under smoky conditions in the eastern Mediterranean. In the remote southeastern Atlantic,

continental African BB plumes appeared to increase boundary-layer CCN concentrations at 0.1–0.4% SS from 50–350 cm^{-3} to 400–1000 cm^{-3} (Kacarab et al., 2020). In the Amazon, $CCN_{0.47\%}$ soared above 4000 cm^{-3} in the presence of transported smoke, which is more than four times the background concentrations reported for that region (Pöhlker et al., 2018). Values of $CCN_{0.325\%}$ increased during BB conditions from 2116 to 3064 cm^{-3} and from 274 to 1189 cm^{-3} over the East Basin of Los Angeles and outflow areas, respectively (Hersey et al., 2013). These concentrations are comparable to those measured at Virginia Key when BB plumes affected the island.

To our knowledge, the last published account of CCN in Florida occurred at Kennedy Space Center (KSC), 320 km northwest of Virginia Key, in 1978 (Radke et al., 1978). At KSC, $CCN_{0.23\%}$ and $CCN_{0.56\%}$ ranged from 660–1350 cm^{-3} and 1848–2140 cm^{-3}, respectively. On "other" days, $CCN_{0.2\%}$ and $CCN_{1.0\%}$ at Virginia Key ranged from 10–5260 cm^{-3} and 10–18 000 cm^{-3}, respectively, which are significantly wider ranges than those observed at KSC. "Other" day $CCN_{0.2\%}$ levels observed at Virginia Key were similar to those reported in Tucson, Arizona (average of 372 cm^{-3} from July–September; Crosbie et al., 2015), and were also in the range observed at four locations in California (Moore et al., 2012). Concentrations of $CCN_{0.4\%}$ measured at relatively rural sites in New York and North Carolina spanned 10–3000 cm^{-3} (Yu et al., 2020), which is a range resembling that observed in this study for $CCN_{0.2\%}$. In comparison to large cities, Virginia Key had significantly lower concentrations. During a haze event in Beijing, $CCN_{0.2\%}$ fluctuated between 2000 and 15 000 cm^{-3} (Zhang et al., 2019) while Burkart et al. (2011) observed background $CCN_{0.5\%}$ ranging from 160–3600 cm^{-3} with an average of 820 cm^{-3} in Vienna, Austria. As mentioned above, Virginia Key is periodically affected by urban aerosols from Miami. However, Miami has little industry relative to other large cities. Thus, even when emissions from Miami reach Virginia Key, it is not surprising CCN concentrations do not rise as high as those in other large cities with more industrial activity.

Although the actual concentrations of CCN are highly variable in various locations around the globe, common themes regarding which air masses influence concentrations in a certain way are evident, especially in the case of smoke. These observations from Virginia Key should be included in global CCN models to assist model predictions for comparable environments and situations. In order to predict CCN concentrations, models rely on information regarding the size distribution, hygroscopicity, and mixing state of the aerosols at altitudes relevant to cloud formation, as well as the degree of SS attained in those clouds (Cubison et al., 2008; Karydis et al., 2011). This work uncovers the remarkable importance of local and distant BB on CCN concentrations in the region, as well as the seeming lack of importance of African dust. Additionally, we reveal that relationships are not straightforward for this location when it comes to heavy precipitation, CCN scavenging, and CCN recharge time. With the help of future work, these findings can be directly connected to which hygroscopic properties or aerosol number concentrations should be used in a CCN model when these same conditions (i.e., African dust events, smoke plumes, and inundant rainfall) materialize in the southeastern U.S.

4. Conclusions

This study investigated the influence of different air mass types on $CCN_{0.2\%}$ and $CCN_{1.0\%}$ concentrations at a ground site in the southeastern U.S. Additionally, we compared ratios of $CCN_{0.2\%}$:$CCN_{1.0\%}$ to gain insight on the hygroscopicity of each air mass. The main findings of this work are as follows:

- $CCN_{0.2\%}$ and $CCN_{1.0\%}$ did not significantly increase during the largest African dust events. Presumably, high dust mass concentrations did not lead to appreciable increases in number concentration as the transported dust particles were relatively large in size but few in number.
- $CCN_{0.2\%}$ and $CCN_{1.0\%}$ increased considerably on days with high influence from BB despite mass concentrations of smoke tracers (i.e., OC and EC) being much lower than African dust concentrations on dust days. Thus, it is assumed the aerosols associated with the smoke events were generally smaller and more numerous than those brought by African dust plumes.
- The ratio of $CCN_{0.2\%}$:$CCN_{1.0\%}$ was similar for all air mass types (0.54 ± 0.17 [dust], 0.55 ± 0.17 [smoke], and 0.55 ± 0.21 [“other”]), except background (0.71 ± 0.14). Background days had some of the highest mass fractions of large and hygroscopic aerosols (e.g., sea salt), which may explain why a larger portion of the CCN on these days were able to activate at the lowest SS.
- Both $CCN_{0.2\%}$ and $CCN_{1.0\%}$ decreased during periods of heavy rainfall. However, $CCN_{0.2\%}$ dropped more rapidly, which may imply larger and/or more hygroscopic aerosols were removed more effectively with precipitation. In support of this, relatively high mass concentrations of sea salt ions (i.e., Na^+ and Cl^-) were observed in precipitation samples during the months relevant to the rain case study shown here.
- The time to restore $CCN_{0.2\%}$ and $CCN_{1.0\%}$ to pre-rain values varied from a few hours to over a day. Such a result warrants further research, in part, so that CCN models can capture this variable behavior in other situations.

Findings from this work can be useful to CCN models for comparable locations. For example, models employed in the southeastern U.S. may not need to account for potential CCN from African dust plumes as heavily as they need to consider those from heighted BB activity in and around the region.

Supplementary Material

Refer to Web version on PubMed Central for supplementary material.

Acknowledgements

The authors acknowledge the NOAA Air Resources Laboratory (ARL) for providing the HYSPLIT transport and dispersion model and all data accessed by the model. They also gratefully acknowledge *earth* (https://earth.nullschool.net/) for its animations of wind conditions at various altitudes. We thank Tom Snowdon for his help in maintaining the CCN and MPL.

Financial Support

This work was funded by NASA grant 80NSSC19K0442 in support of the ACTIVATE Earth Venture Suborbital-3 (EVS-3) investigation, which is funded by NASA's Earth Science Division and managed through the Earth System Science Pathfinder Program Office. South Florida's Cloud-Aerosol-Rain-Observatory, of which the CCN counter and MPL are part, were funded through NSF Major Research Instrumentation grant 092327.

Data availability

Data for daily and monthly mean dust mass concentrations can be found at the University of Miami Data Repository under https://doi.org/10.17604/q3vf-8m31, IMPROVE data are available at http://views.cira.colostate.edu/fed/SiteBrowser/Default.aspx, NADP data can be found at http://nadp.slh.wisc.edu/data/ntn/ntnAllsites.aspx, PERSIANN data are available at http://chrsdata.eng.uci.edu/, and MesoWest data can be found at https://mesowest.utah.edu/. MERRA-2 data can be obtained through NASA GES DISC (https://disc.gsfc.nasa.gov/) and NAAPS data are available at https://www.nrlmry.navy.mil/aerosol/.

References

Abiy AZ, Melesse AM, Abtew W, Whitman D, 2019. Rainfall trend and variability in Southeast Florida: implications for freshwater availability in the Everglades. PloS One 14 (2), e0212008. 10.1371/journal.pone.0212008. [PubMed: 30753221]

Albrecht BA, 1989. Aerosols, cloud microphysics, and fractional cloudiness. Science 245 (4923), 1227–1230. 10.1126/science.245.4923.1227. [PubMed: 17747885]

Aldhaif AM, Lopez DH, Dadashazar H, Sorooshian A, 2020. Sources, frequency, and chemical nature of dust events impacting the United States East Coast. Atmos. Environ 231, 117456. 10.1016/j.atmosenv.2020.117456.

Andreae MO, Rosenfeld D, 2008. Aerosol–cloud–precipitation interactions. Part 1. The nature and sources of cloud-active aerosols. Earth Sci. Rev 89 (1–2), 13–41. 10.1016/j.earscirev.2008.03.001.

Anscombe FJ, 1960. Rejection of outliers. Technometrics 2 (2), 123–146. 10.1080/00401706.1960.10489888.

Barkley AE, Prospero JM, Mahowald N, Hamilton DS, Popendorf KJ, Oehlert AM, Gaston CJ, 2019. African biomass burning is a substantial source of phosphorus deposition to the Amazon, Tropical Atlantic Ocean, and Southern Ocean. Proc. Natl. Acad. Sci. Unit. States Am 116 (33), 16216–16221. 10.1073/pnas.1906091116.

Barnes I, Hjorth J, Mihalopoulos N, 2006. Dimethyl sulfide and dimethyl sulfoxide and their oxidation in the atmosphere. Chem. Rev 106 (3), 940–975. 10.1021/cr020529+. [PubMed: 16522014]

Bègue N, Tulet P, Pelon J, Aouizerats B, Berger A, Schwarzenboeck A, 2015. Aerosol processing and CCN formation of an intense Saharan dust plume during the EUCAARI 2008 campaign. Atmos. Chem. Phys 15 (6), 3497–3516. 10.5194/acp-15-3497-2015.

Blanca MJ, Alarcón R, Arnau J, Bono R, Bendayan R, 2017. Non-normal data: is ANOVA still a valid option? Psicothema 29 (4), 552–557. 10.7334/psicothema2016.383. [PubMed: 29048317]

Bougiatioti A, Bezantakos S, Stavroulas I, Kalivitis N, Kokkalis P, Biskos G, Nenes A, 2016. Biomass-burning impact on CCN number, hygroscopicity and cloud formation during summertime in the eastern Mediterranean. Atmos. Chem. Phys 16 (11), 7389–7409. 10.5194/acp-16-7389-2016.

Bouwman AF, Lee DS, Asman WAH, Dentener FJ, Van Der Hoek KW, Olivier JGJ, 1997. A global high-resolution emission inventory for ammonia. Global Biogeochem. Cycles 11 (4), 561–587. 10.1029/97gb02266.

Brandli HW, Ashman JP, Reinke DL, 1977. Texas dust moves into Florida. Mon. Weather Rev 105 (8), 1068–1070. 10.1175/1520-0493(1977)105<1068:tdmif>2.0.co;2.

Brey SJ, Ruminski M, Atwood SA, Fischer EV, 2018. Connecting smoke plumes to sources using Hazard Mapping System (HMS) smoke and fire location data over North America. Atmos. Chem. Phys 18 (3), 1745–1761. 10.5194/acp-18-1745-2018.

Burkart J, Steiner G, Reischl G, Hitzenberger R, 2011. Long-term study of cloud condensation nuclei (CCN) activation of the atmospheric aerosol in Vienna. Atmos. Environ 45 (32), 5751–5759. 10.1016/j.atmosenv.2011.07.022.

Charlson RJ, Lovelock JE, Andreae MO, Warren SG, 1987. Oceanic phytoplankton, atmospheric sulphur, cloud albedo and climate. Nature 326 (6114), 655–661. 10.1038/326655a0.

Chen L, Li Q, Wu D, Sun H, Wei Y, Ding X, Chen J, 2019. Size distribution and chemical composition of primary particles emitted during open biomass burning processes: impacts on cloud condensation nuclei activation. Sci. Total Environ 674, 179–188. 10.1016/j.scitotenv.2019.03.419. [PubMed: 31004894]

Chesselet R, Morelli J, Buat-Menard P, 1972. Variations in ionic ratios between reference sea water and marine aerosols. J. Geophys. Res 77 (27), 5116–5131. 10.1029/jc077i027p05116.

Chow JC, Lowenthal DH, Chen LWA, Wang X, Watson JG, 2015. Mass reconstruction methods for PM2.5: a review. Air Quality, Atmosphere & Health 8 (3), 243–263. 10.1007/s11869-015-0338-3.

Chuang PY, Collins DR, Pawlowska H, Snider JR, Jonsson HH, Brenguier JL, Seinfeld JH, 2000. CCN measurements during ACE-2 and their relationship to cloud microphysical properties. Tellus B 52 (2), 843–867. 10.1034/j.1600-0889.2000.00018.x.

Clarke A, Kapustin V, Howell S, Moore K, Lienert B, Masonis S, Covert D, 2003. Sea-salt size distributions from breaking waves: implications for marine aerosol production and optical extinction measurements during SEAS. J. Atmos. Ocean. Technol 20 (10), 1362–1374. 10.1175/1520-0426(2003)020<1362:ssdfbw>2.0.co;2.

Clements CB, Zhong S, Bian X, Heilman WE, Byun DW, 2008. First observations of turbulence generated by grass fires. J. Geophys. Res 113 (D22), D22102. 10.1029/2008jd010014.

Cottle P, Strawbridge K, McKendry I, O'Neill N, Saha A, 2013. A pervasive and persistent Asian dust event over North America during spring 2010: lidar and sunphotometer observations. Atmos. Chem. Phys 13 (9), 4515–4527. 10.5194/acp-13-4515-2013.

Crosbie E, Youn JS, Balch B, Wonaschütz A, Shingler T, Wang Z, Sorooshian A, 2015. On the competition among aerosol number, size and composition in predicting CCN variability: a multi-annual field study in an urbanized desert. Atmos. Chem. Phys 15 (12), 6943–6958. 10.5194/acp-15-6943-2015. [PubMed: 26316879]

Cruz MT, Bañaga PA, Betito G, Braun RA, Stahl C, Aghdam MA, Sorooshian A, 2019. Size-resolved composition and morphology of particulate matter during the southwest monsoon in Metro Manila, Philippines. Atmos. Chem. Phys 19 (16), 10675–10696. 10.5194/acp-19-10675-2019.

Cubison MJ, Ervens B, Feingold G, Docherty KS, Ulbrich IM, Shields L, Jimenez JL, 2008. The influence of chemical composition and mixing state of Los Angeles urban aerosol on CCN number and cloud properties. Atmos. Chem. Phys 8 (18), 5649–5667. 10.5194/acp-8-5649-2008.

Cugerone K, De Michele C, Ghezzi A, Gianelle V, 2018. Aerosol removal due to precipitation and wind forcings in Milan urban area. J. Hydrol 556, 1256–1262. 10.1016/j.jhydrol.2017.06.033.

David AS, Jones IM, Lake EC, 2019. Wind speed predicts population dynamics of the eriophyid mite Floracarus perrepae on invasive Old World climbing fern (Lygodium microphyllum) in a shade house colony. Exp. Appl. Acarol 78 (2), 263–272. 10.1007/s10493-019-00391-3. [PubMed: 31177338]

Davy R, 2018. The climatology of the atmospheric boundary layer in contemporary global climate models. J. Clim 31 (22), 9151–9173. 10.1175/jcli-d-17-0498.1.

Delgadillo R, Voss KJ, Zuidema P, 2018. Characteristics of optically thin coastal Florida cumuli derived from surface-based lidar measurements. J. Geophys. Res.: Atmosphere 123 (18), 10,591–510,605. 10.1029/2018JD028867.

Dementeva A, Zhamsueva G, Zayakhanov A, Balzhanov T, 2018. Analysis of transport of smoke aerosol in the atmosphere of the Baikal region by data of NAAPS and CALIPSO. Proc. SPIE 10833, 24th Int. Symp. Atmos. Ocean Opt. Atmos. Phys. 1083377. 10.1117/12.2503059.

Denjean C, Caquineau S, Desboeufs K, Laurent B, Maille M, Quiñones Rosado M, Formenti P, 2015. Long-range transport across the Atlantic in summertime does not enhance the hygroscopicity of African mineral dust. Geophys. Res. Lett 42 (18), 7835–7843. 10.1002/2015GL065693.

Dusek U, Covert DS, Wiedensohler A, Neusüss C, Weise D, Cantrell W, 2003. Cloud condensation nuclei spectra derived from size distributions and hygroscopic properties of the aerosol in coastal south-west Portugal during ACE-2. Tellus B 55 (1), 35–53. 10.3402/tellusb.v55i1.16357.

Gantt B, Kelly JT, Bash JO, 2015. Updating sea spray aerosol emissions in the Community Multiscale Air Quality (CMAQ) model version 5.0.2. Geosci. Model Dev. (GMD) 8 (11), 3733–3746. 10.5194/gmd-8-3733-2015.

Gartman N, 2017. Quality Assurance Report National Atmospheric Deposition Program 2016. http://nadp.slh.wisc.edu/lib/qa/cal_qar_2016.pdf.

Gasparini R, Collins DR, Andrews E, Sheridan PJ, Ogren JA, Hudson JG, 2006. Coupling aerosol size distributions and size-resolved hygroscopicity to predict humidity-dependent optical properties and cloud condensation nuclei spectra. J. Geophys. Res 111 (D5), D05S13. 10.1029/2005jd006092.

Gaston C, Cahill J, Collins D, Suski K, Ge J, Barkley A, Prather K, 2018. The cloud nucleating properties and mixing state of marine aerosols sampled along the southern California coast. Atmosphere 9 (2), 52. 10.3390/atmos9020052.

Gaudichet A, Echalar F, Chatenet B, Quisefit JP, Malingre G, Cachier H, Maenhaut W, 1995. Trace elements in tropical African savanna biomass burning aerosols. J. Atmos. Chem 22 (1–2), 19–39. 10.1007/bf00708179.

Ge C, Wang J, Reid JS, Posselt DJ, Xian P, Hyer E, 2017. Mesoscale modeling of smoke transport from equatorial Southeast Asian Maritime Continent to the Philippines: first comparison of ensemble analysis with in situ observations. J. Geophys. Res.: Atmosphere 122 (10), 5380–5398. 10.1002/2016JD026241.

Gelaro R, McCarty W, Suárez MJ, Todling R, Molod A, Takacs L, Zhao B, 2017. The Modern-Era retrospective analysis for research and Applications, version 2 (MERRA-2). J. Clim. 30 (14), 5419–5454. 10.1175/jcli-d-16-0758.1. [PubMed: 32020988]

Groß S, Esselborn M, Weinzierl B, Wirth M, Fix A, Petzold A, 2013. Aerosol classification by airborne high spectral resolution lidar observations. Atmos. Chem. Phys 13 (5), 2487–2505. 10.5194/acp-13-2487-2013.

Haarig M, Ansmann A, Althausen D, Klepel A, Groß S, Freudenthaler V, Baars H, 2017. Triple-wavelength depolarization-ratio profiling of Saharan dust over Barbados during SALTRACE in 2013 and 2014. Atmos. Chem. Phys 17 (17), 10767–10794. 10.5194/acp-17-10767-2017.

Haarig M, Walser A, Ansmann A, Dollner M, Althausen D, Sauer D, Weinzierl B, 2019. Profiles of cloud condensation nuclei, dust mass concentration, and ice-nucleating-particle-relevant aerosol properties in the Saharan Air Layer over Barbados from polarization lidar and airborne in situ measurements. Atmos. Chem. Phys 19 (22), 13773–13788. 10.5194/acp-19-13773-2019.

Hand JL, Prenni AJ, Schichtel BA, Malm WC, Chow JC, 2019. Trends in remote PM2.5 residual mass across the United States: implications for aerosol mass reconstruction in the IMPROVE network. Atmos. Environ 203, 141–152. 10.1016/j.atmosenv.2019.01.049.

Hand JL, Schichtel BA, Pitchford M, Malm WC, Frank NH, 2012. Seasonal composition of remote and urban fine particulate matter in the United States. J. Geophys. Res.: Atmosphere 117 (D5), D05209. 10.1029/2011jd017122.

Hatch CD, Gierlus KM, Schuttlefield JD, Grassian VH, 2008. Water adsorption and cloud condensation nuclei activity of calcite and calcite coated with model humic and fulvic acids. Atmos. Environ 42 (22), 5672–5684. 10.1016/j.atmosenv.2008.03.005.

Hennigan CJ, Westervelt DM, Riipinen I, Engelhart GJ, Lee T, Collett JL, Robinson AL, 2012. New particle formation and growth in biomass burning plumes: an important source of cloud condensation nuclei. Geophys. Res. Lett 39 (9), L09805. 10.1029/2012gl050930.

Hersey SP, Craven JS, Metcalf AR, Lin J, Lathem T, Suski KJ, Seinfeld JH, 2013. Composition and hygroscopicity of the Los Angeles aerosol: CalNex. J. Geophys. Res.: Atmosphere 118 (7), 3016–3036. 10.1002/jgrd.50307.

Hersey SP, Craven JS, Schilling KA, Metcalf AR, Sorooshian A, Chan MN, Seinfeld JH, 2011. The Pasadena Aerosol Characterization Observatory (PACO): chemical and physical analysis of the western Los Angeles basin aerosol. Atmos. Chem. Phys 11 (15), 7417–7443. 10.5194/acp-11-7417-2011.

Hogan TF, Liu M, Ridout JA, Peng MS, Whitcomb TR, Ruston BC, Reynolds CA, Eckermann SD, Moskaitis JR, Baker NL, McCormack JP, Viner KC, McLay JG, Flatau MK, Xu L, Chen C, Chang SW, 2014. The Navy global environmental model. Oceanography 27 (3), 116–125. 10.5670/oceanog.2014.73.

Hogan TF, Rosmond TE, 1991. The description of the Navy operational global atmospheric prediction system's spectral forecast model. Mon. Weather Rev 119 (8), 1786–1815. 10.1175/1520-0493(1991)119<1786:tdotno>2.0.co;2.

Hoose C, Lohmann U, Bennartz R, Croft B, Lesins G, 2008. Global simulations of aerosol processing in clouds. Atmospheric Chemistry and Physics 8 (23), 6939–6963. 10.5194/acp-8-6939-2008.

Horel J, Splitt M, Dunn L, Pechmann J, White B, Ciliberti C, Burks J, 2002. Mesowest: Cooperative Mesonets in the Western United States. Bull. Am. Meteorol. Soc 83 (2), 211–225. 10.1175/1520-0477(2002)083<0211:MCMITW>2.3.co;2.

Hu PS, Schmitt RR, Nguyen L, Chambers M, Friedman D, Gilmore MM, Wingfield A, 2021. Port Performance Freight Statistics in 2019: Annual Report to Congress 2020. 10.21949/1520450.

Huneeus N, Schulz M, Balkanski Y, Griesfeller J, Prospero J, Kinne S, Zender CS, 2011. Global dust model intercomparison in AeroCom phase I. Atmos. Chem. Phys 11 (15), 7781–7816. 10.5194/acp-11-7781-2011.

IPCC, 2013. Climate Change 2013: The Physical Science Basis. Retrieved from Cambridge, United Kingdom and New York, NY, USA: Cambridge University Press. 10.1017/CBO9781107415324.

Jaffe DA, O'Neill SM, Larkin NK, Holder AL, Peterson DL, Halofsky JE, Rappold AG, 2020. Wildfire and prescribed burning impacts on air quality in the United States. J. Air Waste Manag. Assoc 70 (6), 583–615. 10.1080/10962247.2020.1749731. [PubMed: 32240055]

Kacarab M, Thornhill KL, Dobracki A, Howell SG, O'Brien JR, Freitag S, Nenes A, 2020. Biomass burning aerosol as a modulator of the droplet number in the southeast Atlantic region. Atmos. Chem. Phys 20 (5), 3029–3040. 10.5194/acp-20-3029-2020.

Kandler K, Schneiders K, Ebert M, Hartmann M, Weinbruch S, Prass M, Pöhlker C, 2018. Composition and mixing state of atmospheric aerosols determined by electron microscopy: method development and application to aged Saharan dust deposition in the Caribbean boundary layer. Atmos. Chem. Phys 18 (18), 13429–13455. 10.5194/acp-18-13429-2018.

Karydis VA, Kumar P, Barahona D, Sokolik IN, Nenes A, 2011. On the effect of dust particles on global cloud condensation nuclei and cloud droplet number. J. Geophys. Res.: Atmos 116 (D23), D23204. 10.1029/2011jd016283.

Kavouras IG, Nikolich G, Etyemezian V, Dubois DW, King J, Shafer D, 2012. In situ observations of soil minerals and organic matter in the early phases of prescribed fires. J. Geophys. Res.: Atmos 117 (D12), D12313. 10.1029/2011jd017420.

Keller MD, 1989. Dimethyl sulfide production and marine phytoplankton: the importance of species composition and cell size. Biol. Oceanogr 6 (5–6), 375–382. 10.1080/01965581.1988.10749540.

Khan AL, Klein AG, Katich JM, Xian P, 2019. Local emissions and regional wildfires influence refractory black carbon observations near palmer station, Antarctica. Front. Earth Sci 7 (49), 1–8. 10.3389/feart.2019.00049.

Kitto ME, Anderson DL, 1988. The use of Whatman-41 filters for particle. Atmos. Environ 22 (11), 2629–2630. 10.1016/0004-6981(88)90500-8.

Klejnowski K, Krasa A, Rogula-Kozłowska W, Błaszczak B, 2013. Number size distribution of ambient particles in a typical urban site: the first polish assessment based on long-term (9 Months) measurements. Sci. World J 2013 (539568), 1–13. 10.1155/2013/539568, 2013.

Kramer S, Kirtman B, Zuidema P, Ngan F, 2020a. Subseasonal variability of elevated dust concentrations over south Florida. J. Geophys. Res.: Atmosphere 125 (6), e2019JD031874. 10.1029/2019jd031874.

Kramer SJ, Alvarez C, Barkley A, Colarco PR, Custals L, Delgadillo R, Zuidema P, 2020b. Apparent dust size discrepancy in aerosol reanalysis in north African dust after long-range transport. Atmos. Chem. Phys. Discuss. 20, 10047–10062. 10.5194/acp-20-10047-2020.

Kreidenweis SM, Remer LA, Bruintjes R, Dubovik O, 2001. Smoke aerosol from biomass burning in Mexico: hygroscopic smoke optical model. J. Geophys. Res.: Atmosphere 106 (D5), 4831–4844. 10.1029/2000jd900488.

Kumar P, Sokolik IN, Nenes A, 2011. Measurements of cloud condensation nuclei activity and droplet activation kinetics of fresh unprocessed regional dust samples and minerals. Atmos. Chem. Phys 11 (7), 3527–3541. 10.5194/acp-11-3527-2011.

Kummu M, de Moel H, Salvucci G, Viviroli D, Ward PJ, Varis O, 2016. Over the hills and further away from coast: global geospatial patterns of human and environment over the 20th–21st centuries. Environ. Res. Lett 11 (3), 034010. 10.1088/1748-9326/11/3/034010.

Le Blond JS, Woskie S, Horwell CJ, Williamson BJ, 2017. Particulate matter produced during commercial sugarcane harvesting and processing: a respiratory health hazard? Atmos. Environ 149, 34–46. 10.1016/j.atmosenv.2016.11.012.

Lee S, Ghim YS, Kim S-W, Yoon S-C, 2010. Effect of biomass burning and regional background aerosols on CCN activity derived from airborne in-situ measurements. Atmos. Environ 44 (39), 5227–5236. 10.1016/j.atmosenv.2010.08.044.

Levin Z, Ganor E, Gladstein V, 1996. The effects of desert particles coated with sulfate on rain formation in the eastern mediterranean. J. Appl. Meteorol 35 (9), 1511–1523. 10.1175/1520-0450(1996)035<1511:teodpc>2.0.co;2.

Li-Jones X, Prospero JM, 1998. Variations in the size distribution of non-sea-salt sulfate aerosol in the marine boundary layer at Barbados: impact of African dust. J. Geophys. Res.: Atmosphere 103 (D13), 16073–16084. 10.1029/98jd00883.

Li C, Hu Y, Chen J, Ma Z, Ye X, Yang X, Mellouki A, 2016. Physiochemical properties of carbonaceous aerosol from agricultural residue burning: density, volatility, and hygroscopicity. Atmos. Environ 140, 94–105. 10.1016/j.atmosenv.2016.05.052.

Liu Y, Goodrick SL, Stanturf JA, 2013. Future U.S. wildfire potential trends projected using a dynamically downscaled climate change scenario. For. Ecol. Manag 294, 120–135. 10.1016/j.foreco.2012.06.049.

Lopez D, Rabbani M, Crosbie E, Raman A, Arellano A, Sorooshian A, 2015. Frequency and character of extreme aerosol events in the southwestern United States: a case study analysis in Arizona. Atmosphere 7 (1), 1. 10.3390/atmos7010001. [PubMed: 27088005]

Luan T, Guo X, Zhang T, Guo L, 2019. Below-cloud aerosol scavenging by different-intensity rains in beijing city. J. Meteorol. Res 33 (1), 126–137. 10.1007/s13351-019-8079-0.

Ma S, Karkee M, Scharf PA, Zhang Q, 2014. Sugarcane harvester technology: a critical overview. Appl. Eng. Agric 30 (5), 727–739. 10.13031/aea.30.10696.

Manktelow PT, Carslaw KS, Mann GW, Spracklen DV, 2010. The impact of dust on sulfate aerosol, CN and CCN during an East Asian dust storm. Atmospheric Chemistry and Physics 10 (2), 365–382. 10.5194/acp-10-365-2010.

Markowicz KM, Lisok J, Xian P, 2017. Simulations of the effect of intensive biomass burning in July 2015 on Arctic radiative budget. Atmos. Environ 171, 248–260. 10.1016/j.atmosenv.2017.10.015.

Maudlin LC, Wang Z, Jonsson HH, Sorooshian A, 2015. Impact of wildfires on size-resolved aerosol composition at a coastal California site. Atmos. Environ 119, 59–68. 10.1016/j.atmosenv.2015.08.039.

McCarty J, Justice C, Korontzi S, 2007. Agricultural burning in the Southeastern United States detected by MODIS. Rem. Sens. Environ 108 (2), 151–162. 10.1016/j.rse.2006.03.020.

McKendry IG, Strawbridge KB, O'Neill NT, Macdonald AM, Liu PSK, Leaitch WR, Westphal DL, 2007. Trans-Pacific transport of Saharan dust to western North America: a case study. J. Geophys. Res 112 (D1), D01103. 10.1029/2006jd007129.

Mei F, Hayes PL, Ortega A, Taylor JW, Allan JD, Gilman J, Wang J, 2013. Droplet activation properties of organic aerosols observed at an urban site during CalNex-LA. J. Geophys. Res.: Atmosphere 118 (7), 2903–2917. 10.1002/jgrd.50285.

Middleton NJ, Goudie AS, 2001. Saharan dust: sources and trajectories. Trans. Inst. Br. Geogr 26 (2), 165–181. 10.1111/1475-5661.00013.

Miller J, 1991. Short report: reaction time analysis with outlier exclusion: bias varies with sample size. Quart. J. Exp. Psychol. Sec. A 43 (4), 907–912. 10.1080/14640749108400962.

Molina LT, Kolb CE, De Foy B, Lamb BK, Brune WH, Jimenez JL, Molina MJ, 2007. Air quality in North America's most populous city – overview of the MCMA-2003 campaign. Atmos. Chem. Phys 7 (10), 2447–2473. 10.5194/acp-7-2447-2007.

Molod A, Salmun H, Marquardt Collow AB, 2019. Annual cycle of planetary boundary layer heights estimated from wind profiler network data. J. Geophys. Res.: Atmosphere 124 (12), 6207–6221. 10.1029/2018jd030102.

Moore RH, Cerully K, Bahreini R, Brock CA, Middlebrook AM, Nenes A, 2012. Hygroscopicity and composition of California CCN during summer 2010. J. Geophys. Res.: Atmosphere 117 (D21), D00V12. 10.1029/2011jd017352.

Nguyen P, Shearer EJ, Tran H, Ombadi M, Hayatbini N, Palacios T, Sorooshian S, 2019. The CHRS Data Portal, an easily accessible public repository for PERSIANN global satellite precipitation data. Scientific data 6 (1), 1–10. 10.1038/sdata.2018.296. [PubMed: 30647409]

Nolte CG, Appel KW, Kelly JT, Bhave PV, Fahey KM, Collett JL Jr., Young JO, 2015. Evaluation of the Community Multiscale Air Quality (CMAQ) model v5.0 against size-resolved measurements of inorganic particle composition across sites in North America. Geosci. Model Dev. (GMD) 8 (9), 2877–2892. 10.5194/gmd-8-2877-2015.

Ohata S, Moteki N, Mori T, Koike M, Kondo Y, 2016. A key process controlling the wet removal of aerosols: new observational evidence. Sci. Rep 6 (1), 34113. 10.1038/srep34113. [PubMed: 27703169]

Palmer TY, 1981. Large fire winds, gases and smoke. Atmos. Environ 15 (10–11), 2079–2090. 10.1016/0004-6981(81)90241-9.

Perry KD, Cahill TA, Eldred RA, Dutcher DD, Gill TE, 1997. Long-range transport of North African dust to the eastern United States. J. Geophys. Res.: Atmosphere 102 (D10), 11225–11238. 10.1029/97jd00260.

Petters MD, Kreidenweis SM, 2007. A single parameter representation of hygroscopic growth and cloud condensation nucleus activity. Atmos. Chem. Phys 7 (8), 1961–1971. 10.5194/acp-7-1961-2007.

Pöhlker ML, Ditas F, Saturno J, Klimach T, Hrabě de Angelis I, Araùjo AC, Pöhlker C, 2018. Long-term observations of cloud condensation nuclei over the Amazon rain forest – Part 2: variability and characteristics of biomass burning, long-range transport, and pristine rain forest aerosols. Atmos. Chem. Phys 18 (14), 10289–10331. 10.5194/acp-18-10289-2018.

Popovicheva O, Kistler M, Kireeva E, Persiantseva N, Timofeev M, Kopeikin V, Kasper-Giebl A, 2014. Physicochemical characterization of smoke aerosol during large-scale wildfires: extreme event of August 2010 in Moscow. Atmos. Environ 96, 405–414. 10.1016/j.atmosenv.2014.03.026.

Pringle KJ, Tost H, Pozzer A, Pöschl U, Lelieveld J, 2010. Global distribution of the effective aerosol hygroscopicity parameter for CCN activation. Atmospheric Chemistry and Physics 10 (12), 5241–5255. 10.5194/acp-10-5241-2010.

Prospero JM, 1999. Long-term measurements of the transport of African mineral dust to the southeastern United States: implications for regional air quality. J. Geophys. Res.: Atmosphere 104 (D13), 15917–15927. 10.1029/1999jd900072.

Prospero JM, Collard F-X, Molinié J, Jeannot A, 2014. Characterizing the annual cycle of African dust transport to the Caribbean Basin and South America and its impact on the environment and air quality. Global Biogeochem. Cycles 28 (7), 757–773. 10.1002/2013gb004802.

Prospero JM, Glaccum RA, Nees RT, 1981. Atmospheric transport of soil dust from Africa to South America. Nature 289 (5798), 570–572. 10.1038/289570a0.

Qi M, Jiang L, Liu Y, Xiong Q, Sun C, Li X, Yang X, 2018. Analysis of the characteristics and sources of carbonaceous aerosols in PM2.5 in the Beijing, Tianjin, and Langfang region, China. Int. J. Environ. Res. Publ. Health 15 (7), 1483. 10.3390/ijerph15071483.

Quinn PK, Bates TS, 2014. Ocean Derived Aerosol and Its Climate Impacts in Treatise on Geochemistry, Second Edition. Elsevier, pp. 317–330. 10.1016/b978-0-08-095975-7.00416-2.

Radke LF, Langer G, Hindman EE, 1978. Airborne Measurements of Cloud Forming Nuclei and Aerosol Particles at Kennedy Space Center. NASA Contractor Report (CR)-160359..

Ramírez-Romero C, Jaramillo A, Córdoba MF, Raga GB, Miranda J, Alvarez-Ospina H, Ladino LA, 2021. African dust particles over the western Caribbean – Part I: impact on air quality over the Yucatán Peninsula. Atmos. Chem. Phys 21 (1), 239–253. 10.5194/acp-21-239-2021.

Rissler J, Swietlicki E, Zhou J, Roberts G, Andreae MO, Gatti LV, Artaxo P, 2004. Physical properties of the sub-micrometer aerosol over the Amazon rain forest during the wet-to-dry season

transition - comparison of modeled and measured CCN concentrations. Atmos. Chem. Phys 4 (8), 2119–2143. 10.5194/acp-4-2119-2004.

Roberts GC, Nenes A, 2005. A continuous-flow streamwise thermal-gradient CCN chamber for atmospheric measurements. Aerosol. Sci. Technol 39 (3), 206–221. 10.1080/027868290913988.

Rocha-Lima A, Martins JV, Remer LA, Todd M, Marsham JH, Engelstaedter S, Washington R, 2018. A detailed characterization of the Saharan dust collected during the Fennec campaign in 2011: in situ ground-based and laboratory measurements. Atmos. Chem. Phys 18 (2), 1023–1043. 10.5194/acp-18-1023-2018.

Rolph G, Stein A, Stunder B, 2017. Real-time Environmental Applications and Display sYstem: READY. Environ. Model. Software 95, 210–228. 10.1016/j.envsoft.2017.06.025.

Rosenfeld D, Lohmann U, Raga GB, O'Dowd CD, Kulmala M, Fuzzi S, Andreae MO, 2008. Flood or drought: how do aerosols affect precipitation? Science 321 (5894), 1309–1313. 10.1126/science.1160606. [PubMed: 18772428]

Roy A, Choi Y, Souri AH, Jeon W, Diao L, Pan S, Westenbarger D, 2018. Effects of biomass burning emissions on air quality over the continental USA: a three-year comprehensive evaluation accounting for sensitivities due to boundary conditions and plume rise height. In: Gupta T, Agarwal AK, Agarwal RA, Labhsetwar NK (Eds.), Environmental Contaminants: Measurement, Modelling and Control. Springer Singapore, Singapore, 245–278. 10.1007/978-981-10-7332-8_12.

Schlosser JS, Braun RA, Bradley T, Dadashazar H, MacDonald AB, Aldhaif AA, Sorooshian A, 2017. Analysis of aerosol composition data for western United States wildfires between 2005 and 2015: dust emissions, chloride depletion, and most enhanced aerosol constituents. J. Geophys. Res.: Atmosphere 122 (16), 8951–8966. 10.1002/2017JD026547.

Schlosser JS, Dadashazar H, Edwards EL, Hossein Mardi A, Prabhakar G, Stahl C, Sorooshian A, 2020. Relationships between supermicrometer sea salt aerosol and marine boundary layer conditions: insights from repeated identical flight patterns. J. Geophys. Res.: Atmosphere 125 (12). 10.1029/2019jd032346.

Schulze BC, Wallace HW, Bui AT, Flynn JH, Erickson MH, Alvarez S, Griffin RJ, 2018. The impacts of regional shipping emissions on the chemical characteristics of coastal submicron aerosols near Houston, TX. Atmos. Chem. Phys 18 (19), 14217–14241. 10.5194/acp-18-14217-2018.

Sevimoğlu O, Rogge WF, 2015. Organic compound concentrations of size-segregated PM10 during sugarcane burning and growing seasons at a rural and an urban site in Florida, USA. Aerosol Air Qual. Res 15 (5), 1720–1736. 10.4209/aaqr.2015.02.0069.

Sevimoğlu O, Rogge WF, 2016. Seasonal size-segregated PM10 and PAH concentrations in a rural area of sugarcane agriculture versus a coastal urban area in Southeastern Florida, USA. Particuology 28, 52–59. 10.1016/j.partic.2015.09.013.

Sevimoğlu O, Rogge WF, 2019. Seasonal variations of PM10 — trace elements, PAHs and Levoglucosan: rural sugarcane growing area versus coastal urban area in Southeastern Florida, USA. Part II: elemental concentrations. Particuology 46, 99–108. 10.1016/j.partic.2019.05.001.

Smith DB, Demetriades A, De Caritat P, Wang X, 2019. The history, progress, and future of global-scale geochemical mapping. Geochim. Bras 32 (2), 115–135. 10.21715/GB2358-2812.2018322115.

Sotiropoulou R-EP, Nenes A, Adams PJ, Seinfeld JH, 2007. Cloud condensation nuclei prediction error from application of Köhler theory: importance for the aerosol indirect effect. J. Geophys. Res 112 (D12), D12202. 10.1029/2006jd007834.

Stein AF, Draxler RR, Rolph GD, Stunder BJB, Cohen MD, Ngan F, 2015. NOAA's HYSPLIT atmospheric transport and dispersion modeling System. Bull. Am. Meteorol. Soc 96 (12), 2059–2077. 10.1175/bams-d-14-00110.1.

Stroud CA, Nenes A, Jimenez JL, Decarlo PF, Huffman JA, Bruintjes R, Nandi S, 2007. Cloud activating properties of aerosol observed during CELTIC. J. Atmos. Sci 64 (2), 441–459. 10.1175/jas3843.1.

Sturtz TM, Schichtel BA, Larson TV, 2014. Coupling chemical transport model source attributions with positive matrix factorization: application to two IMPROVE sites impacted by wildfires. Environ. Sci. Technol 48 (19), 11389–11396. 10.1021/es502749r. [PubMed: 25181558]

Sullivan RC, Moore MJK, Petters MD, Kreidenweis SM, Roberts GC, Prather KA, 2009. Effect of chemical mixing state on the hygroscopicity and cloud nucleation properties of calcium mineral dust particles. Atmos. Chem. Phys 9 (10), 3303–3316. 10.5194/acp-9-3303-2009.

Szidat S, Ruff M, Perron N, Wacker L, Synal HA, Hallquist M, Simpson D, 2009. Fossil and non-fossil sources of organic carbon (OC) and elemental carbon (EC) in Göteborg, Sweden. Atmos. Chem. Phys 9 (5), 1521–1535. 10.5194/acp-9-1521-2009.

Twomey S, 1974. Pollution and the planetary albedo. Atmos. Environ 8 (12), 1251–1256. 10.1016/0004-6981(74)90004-3.

United Nations, Department of Economic and Social Affairs, Population Division, 2019. World Urbanization Prospects: the 2018 Revision. United Nations, New York.

Vanreken TM, 2003. Toward aerosol/cloud condensation nuclei (CCN) closure during CRYSTAL-FACE. J. Geophys. Res 108 (D20), 4633. 10.1029/2003jd003582.

Wang J, Christopher SA, 2006. Mesoscale modeling of Central American smoke transport to the United States: 2. Smoke radiative impact on regional surface energy budget and boundary layer evolution. J. Geophys. Res.: Atmosphere 111 (D14), D14S92. 10.1029/2005JD006720.

Wang J, Christopher SA, Nair US, Reid JS, Prins EM, Szykman J, Hand JL, 2006. Mesoscale modeling of Central American smoke transport to the United States: 1. “Top-down” assessment of emission strength and diurnal variation impacts. J. Geophys. Res 111 (D5), D05S17. 10.1029/2005jd006416.

Weinzierl B, Ansmann A, Prospero JM, Althausen D, Benker N, Chouza F, Walser A, 2017. The saharan aerosol long-range transport and aerosol–cloud-interaction experiment: overview and selected highlights. Bull. Am. Meteorol. Soc 98 (7), 1427–1451. 10.1175/bams-d-15-00142.1.

Wells KC, Witek M, Flatau P, Kreidenweis SM, Westphal DL, 2007. An analysis of seasonal surface dust aerosol concentrations in the western US (2001–2004): observations and model predictions. Atmos. Environ 41 (31), 6585–6597. 10.1016/j.atmosenv.2007.04.034.

Winer B, Brown D, Michels V, 1991. Statistical Principles in Experimental Design. McGraw-Hill, New York. Winer, B., Brown, D., Michels, V., 1991. Statistical Principles in Experimental Design. McGraw-Hill, New York.

Wu Y, Han Z, Nazmi C, Gross B, Moshary F, 2015. A trans-Pacific Asian dust episode and its impacts to air quality in the east coast of. U.S. Atmos. Environ 106, 358–368. 10.1016/j.atmosenv.2015.02.013.

Xian P, Reid JS, Atwood SA, Johnson RS, Hyer EJ, Westphal DL, Sessions W, 2013. Smoke aerosol transport patterns over the Maritime Continent. Atmos. Res 122, 469–485. 10.1016/j.atmosres.2012.05.006.

Yokelson RJ, Crounse JD, Decarlo PF, Karl T, Urbanski S, Atlas E, Shetter R, 2009. Emissions from biomass burning in the Yucatan. Atmos. Chem. Phys 9 (15), 5785–5812. 10.5194/acp-9-5785-2009.

Yu F, Luo G, Nair AA, Schwab JJ, Sherman JP, Zhang Y, 2020. Wintertime new particle formation and its contribution to cloud condensation nuclei in the Northeastern United States. Atmos. Chem. Phys 20 (4), 2591–2601. 10.5194/acp-20-2591-2020.

Zamora LM, Prospero JM, Hansell DA, 2011. Organic nitrogen in aerosols and precipitation at Barbados and Miami: implications regarding sources, transport and deposition to the western subtropical North Atlantic. J. Geophys. Res.: Atmosphere 116 (D20), D20309. 10.1029/2011JD015660.

Zamora LM, Prospero JM, Hansell DA, Trapp JM, 2013. Atmospheric P deposition to the subtropical North Atlantic: sources, properties, and relationship to N deposition. J. Geophys. Res.: Atmosphere 118 (3), 1546–1562. 10.1002/jgrd.50187.

Zhang F, Ren J, Fan T, Chen L, Xu W, Sun Y, Li Z, 2019. Significantly enhanced aerosol CCN activity and number concentrations by nucleation-initiated haze events: a case study in urban beijing. J. Geophys. Res.: Atmosphere 124 (24), 14102–14113. 10.1029/2019JD031457.

Zheng G, Sedlacek AJ, Aiken AC, Feng Y, Watson TB, Raveh-Rubin S, Wang J, 2020. Long-range transported North American wildfire aerosols observed in marine boundary layer of eastern North Atlantic. Environ. Int 139, 105680. 10.1016/j.envint.2020.105680. [PubMed: 32272293]

Zuidema P, Alvarez C, Kramer SJ, Custals L, Izaguirre M, Sealy P, Blades E, 2019. Is summer african dust arriving earlier to Barbados? The updated long-term in situ dust mass concentration time series from ragged point, Barbados, and Miami, Florida. Bull. Am. Meteorol. Soc 100 (10), 1981–1986. 10.1175/BAMS-D-18-0083.1.

Further reading

Rose D, Gunthe SS, Mikhailov E, Frank GP, Dusek U, Andreae MO, Poschl U, 2008. Calibration and measurement uncertainties of a continuous-flow cloud condensation nuclei counter (DMT-CCNC): CCN activation of ammonium sulfate and sodium chloride aerosol particles in theory and experiment. Atmos. Chem. Phys 8 (5), 1153–1179. 10.5194/acp-8-1153-2008.

HIGHLIGHTS

- African dust plumes do not perturb CCN concentrations in southeast Florida.
- CCN concentrations are greatly increased on days influenced by biomass burning.
- Heavy rainfall reduces CCN concentrations.
- The duration varies for CCN concentrations to restore after periods of heavy rain.

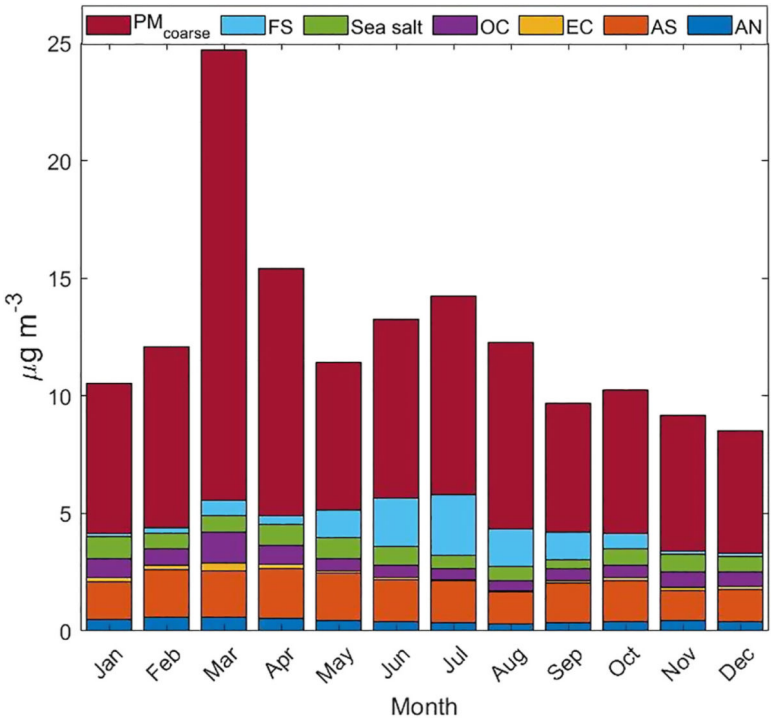

Fig. 1.

Monthly profiles of $PM_{2.5}$ speciation and PM_{coarse} for the EVER1 IMPROVE site based on data from all months in 2013, 2017, and 2018. Six major constituents of $PM_{2.5}$ are presented: FS (fine soil), sea salt, OC (organic carbon), EC (elemental carbon), AS (ammonium sulfate), and AN (ammonium nitrate).

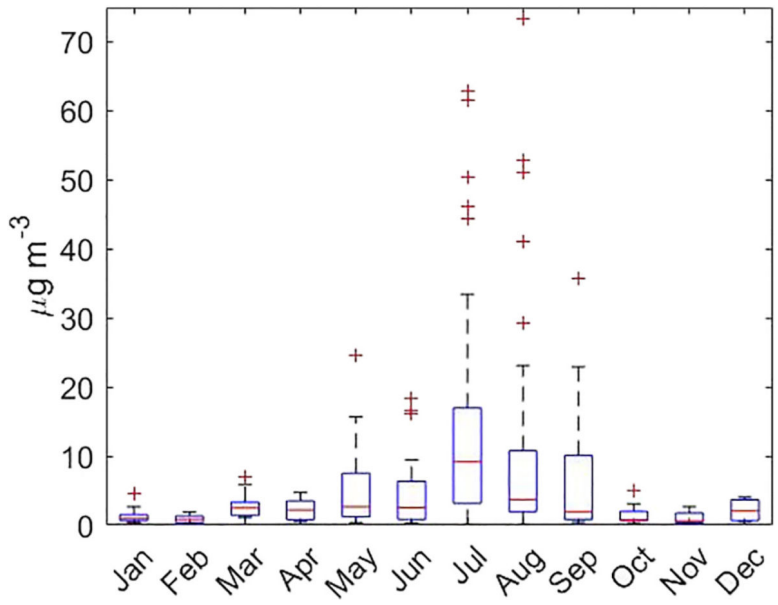

Fig. 2.

Monthly statistics of the African dust mass concentrations measured at the CARObb station in 2013, 2017, and 2018. The red line in the center of each box represents the median, the edges of each box indicate the 25th and 75th quartiles, and red crosses belong to outliers lying in the fourth quartile.

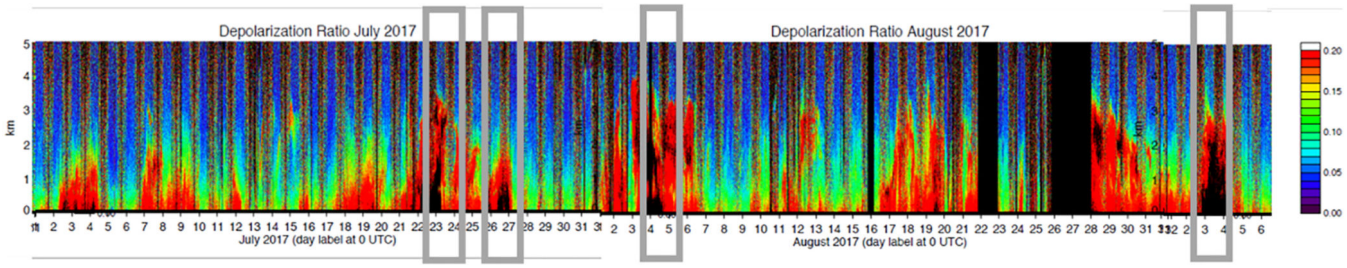

Fig. 3.

Micropulse lidar (MPL) depolarization ratio profile for the summer to early fall (01 July – 06 Sep) of 2017. All of the identified dust days (based on Table 2) occurred within the time period shown above and are indicated by the grey rectangles. Solid black segments (e.g., visible in late August) reflect periods when power was not available for the MPL.

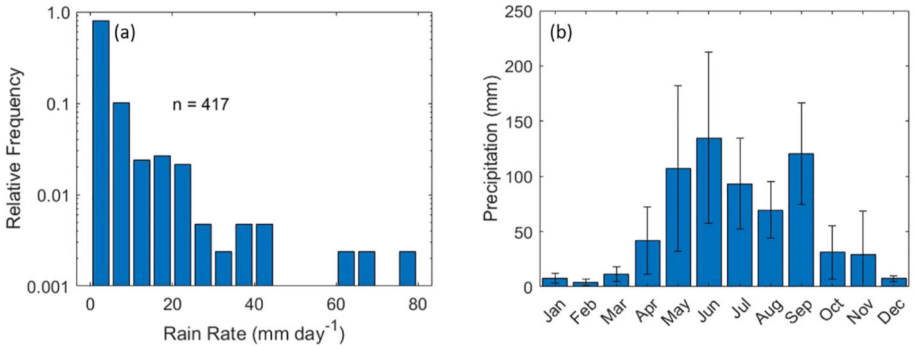

Fig. 4.

(a) Histogram of the daily rain rates and **(b)** monthly mean precipitation accumulation with error bars representing one standard deviation. These results are based on data in 2013, 2017, and 2018.

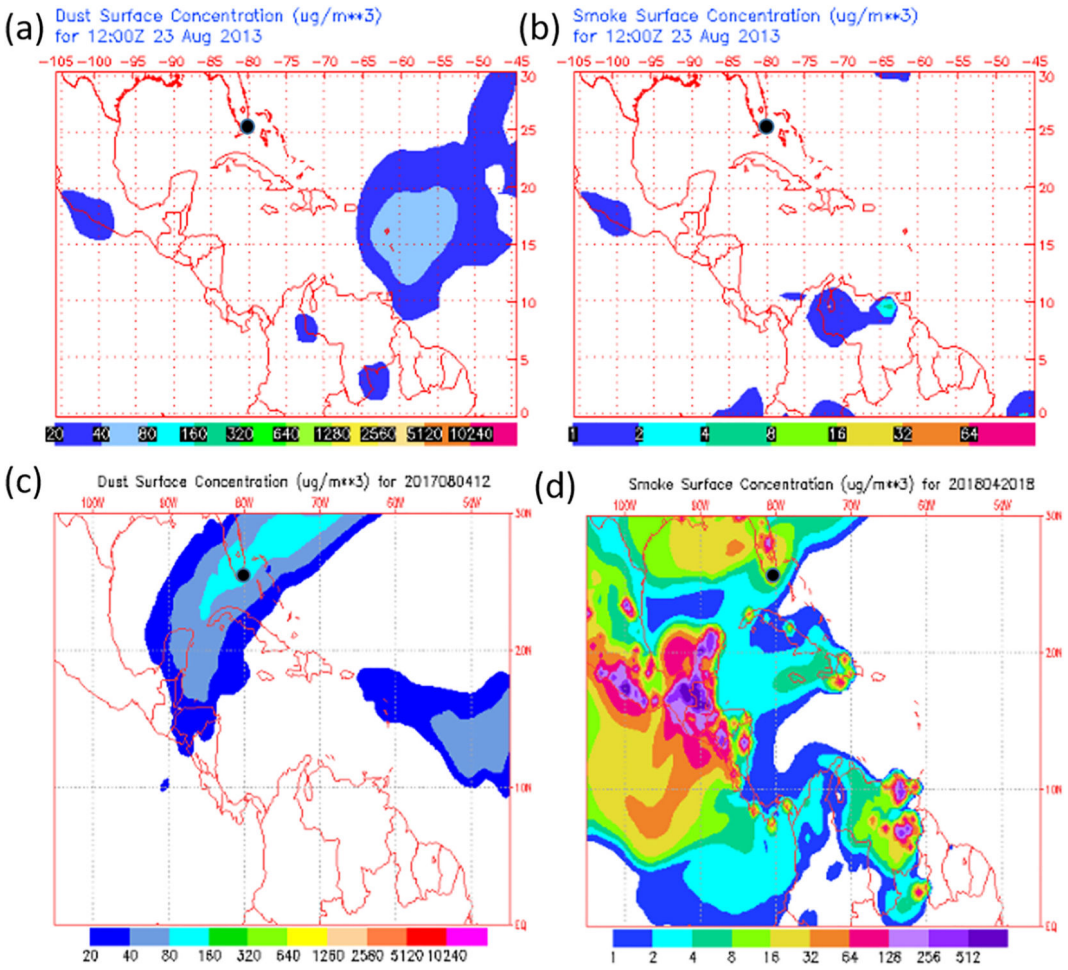

Fig. 5.

NAAPS surface concentrations of (**a**) dust and (**b**) smoke on one of the background days (August 23, 2013), (**c**) dust on the highest dust day (August 4, 2017), (**d**) and smoke on one of the smoke days (April 20, 2018). Virginia Key is marked by a black circular marker.

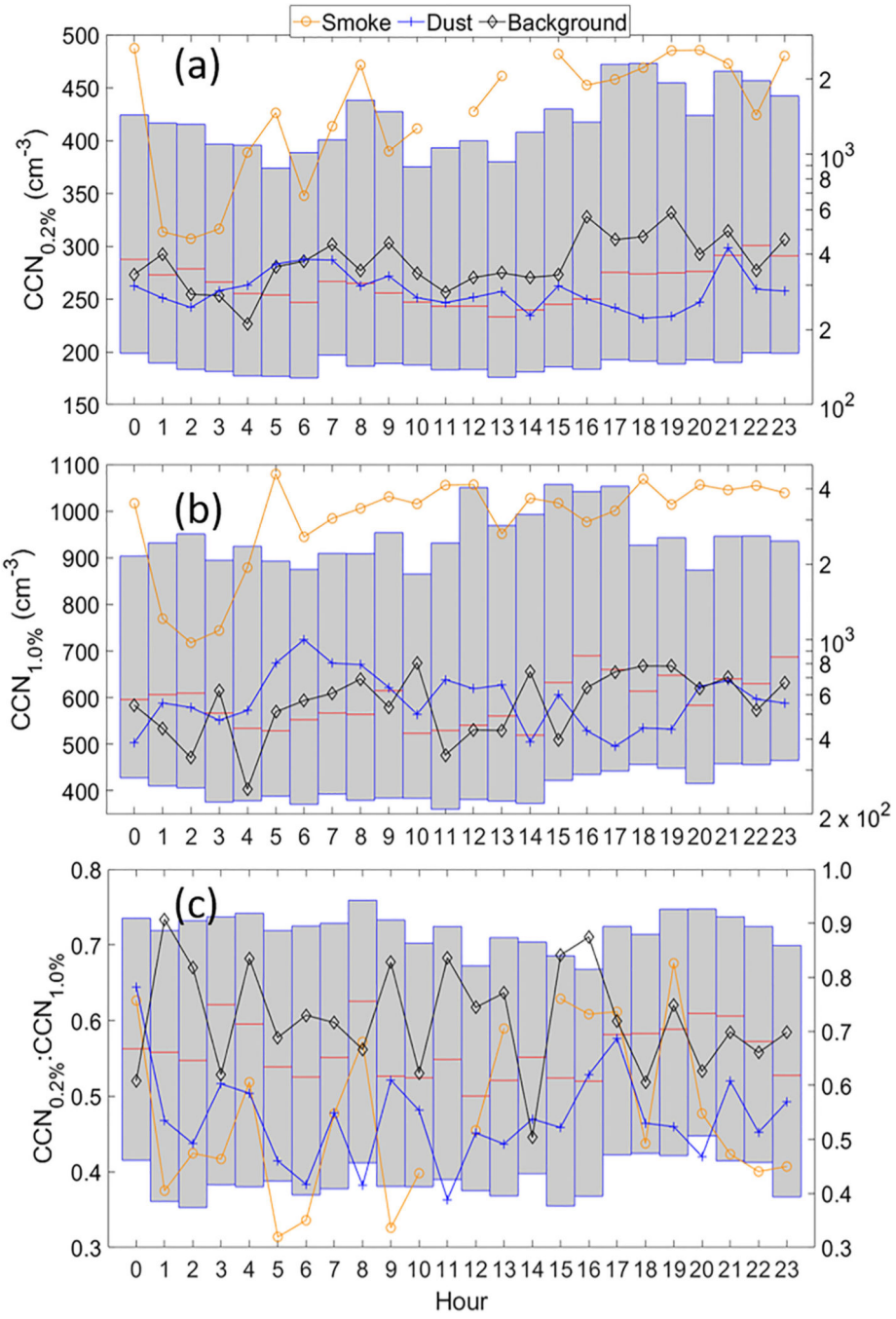

Fig. 6.

Diurnal statistics for (**a**) $CCN_{0.2\%}$, (**b**) $CCN_{1.0\%}$, and (**c**) $CCN_{0.2\%}$:$CCN_{1.0\%}$ for the three categories listed in Table 2. The grey bars, which represent statistics for all 315 days in the study, are shown to contrast with values for each category. The red horizontal lines in each grey bar designate the median, while the bottom and top of the bars mark the 25th and 75th percentiles, respectively, at that given hour. The right y-axis applies to the smoke, dust, and background categories; the left y-axis applies to the grey bars only.

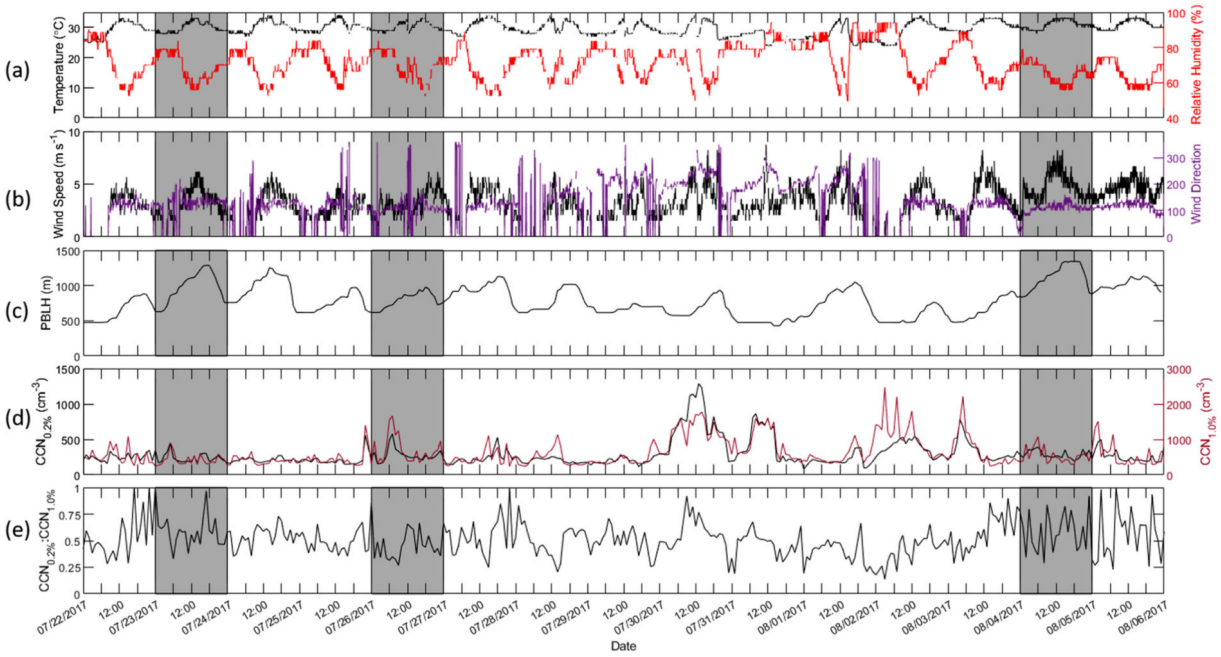

Fig. 7.

Time series of the (**a**) temperature and relative humidity (RH), (**b**) near-surface wind speed and near-surface wind direction, (**c**) planetary boundary layer height (PBLH), (**d**) $CCN_{0.2\%}$ and $CCN_{1.0\%}$, and (**e**) ratio of $CCN_{0.2\%}$:$CCN_{1.0\%}$ during three of the dust days (shaded grey) from Table 2. The lines in the plots correspond to the variable written in the same colored font on either the left or right y-axis of that plot. The amounts of dust occurring on the three dust days shown, from left to right, are 50.36, 33.42, and 73.32 μg m^{-3}.

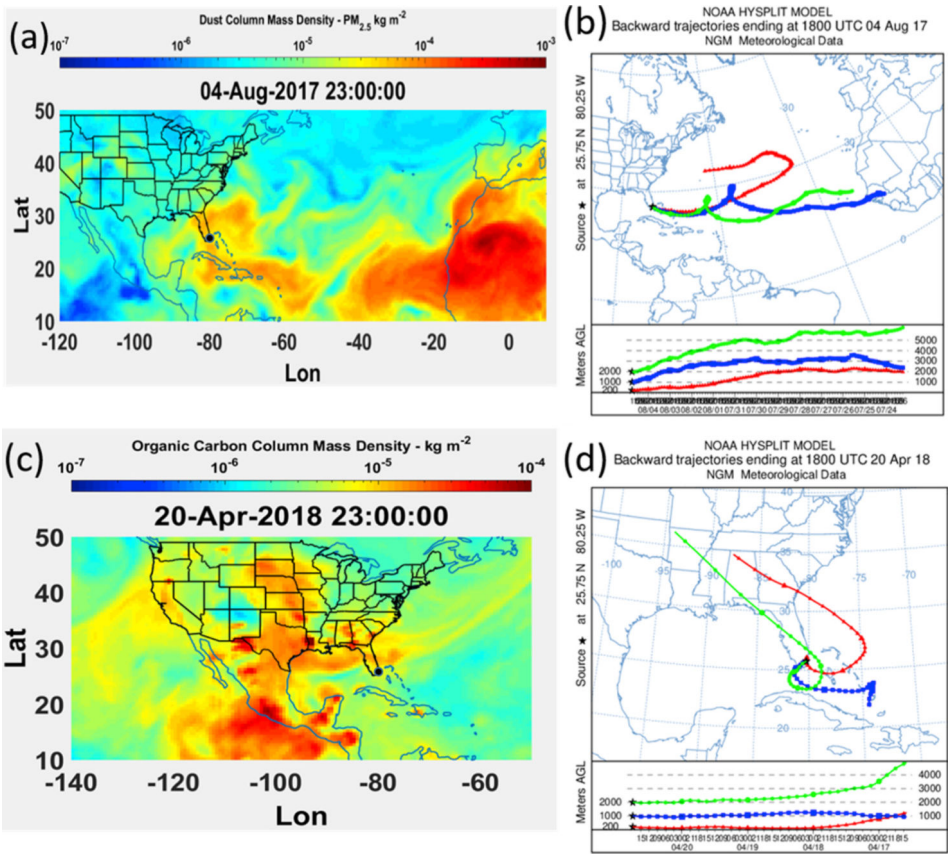

Fig. 8.

(**a**) MERRA-2 fine dust column mass density and (**b**) HYSPLIT 300 h back trajectories ending at CARObon the highest dust concentration day (August 4, 2017). (**c**) MERRA-2 organic carbon column mass density and (**d**) 100 h back trajectories ending at CARObon one of the smoke days (April 20, 2018). Virginia Key is marked by a black circular marker in (**a**) and (**c**).

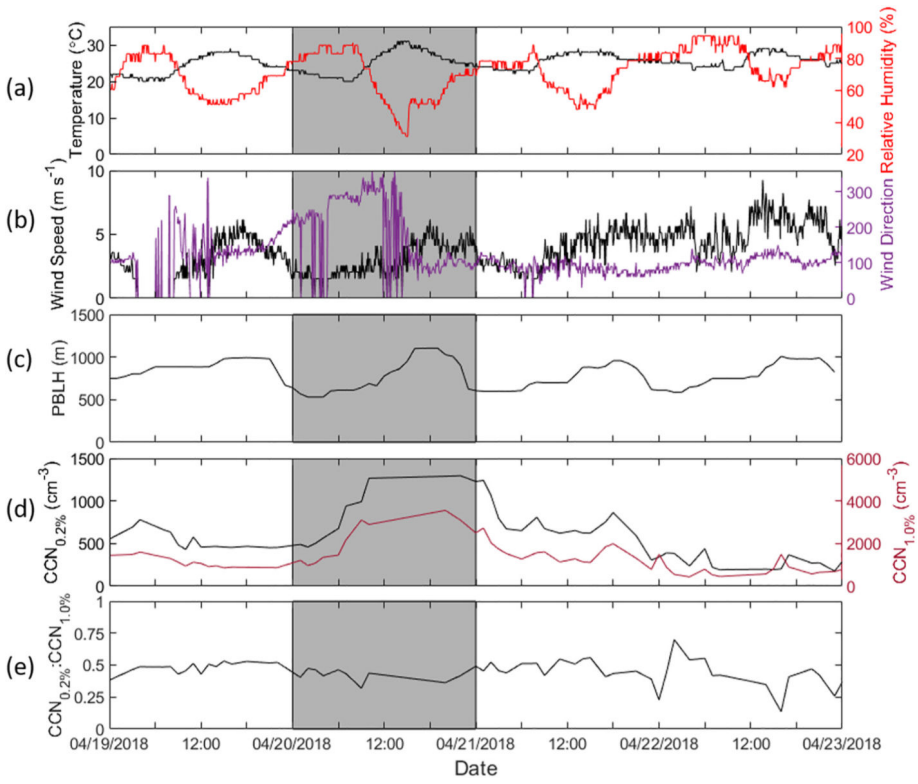

Fig. 9.

Time series of the (**a**) temperature and RH, (**b**) near-surface wind speed and near-surface wind direction, (**c**) PBLH, (**d**) $CCN_{0.2\%}$ and $CCN_{1.0\%}$, and (**e**) ratio of $CCN_{0.2\%}$:$CCN_{1.0\%}$ from April 19, 2018 to April 23, 2018. The lines in the plots correspond to the variable written in the same colored font on either the left or right y-axis. The day shaded in grey was classified as one of the smoke days (April 20, 2018).

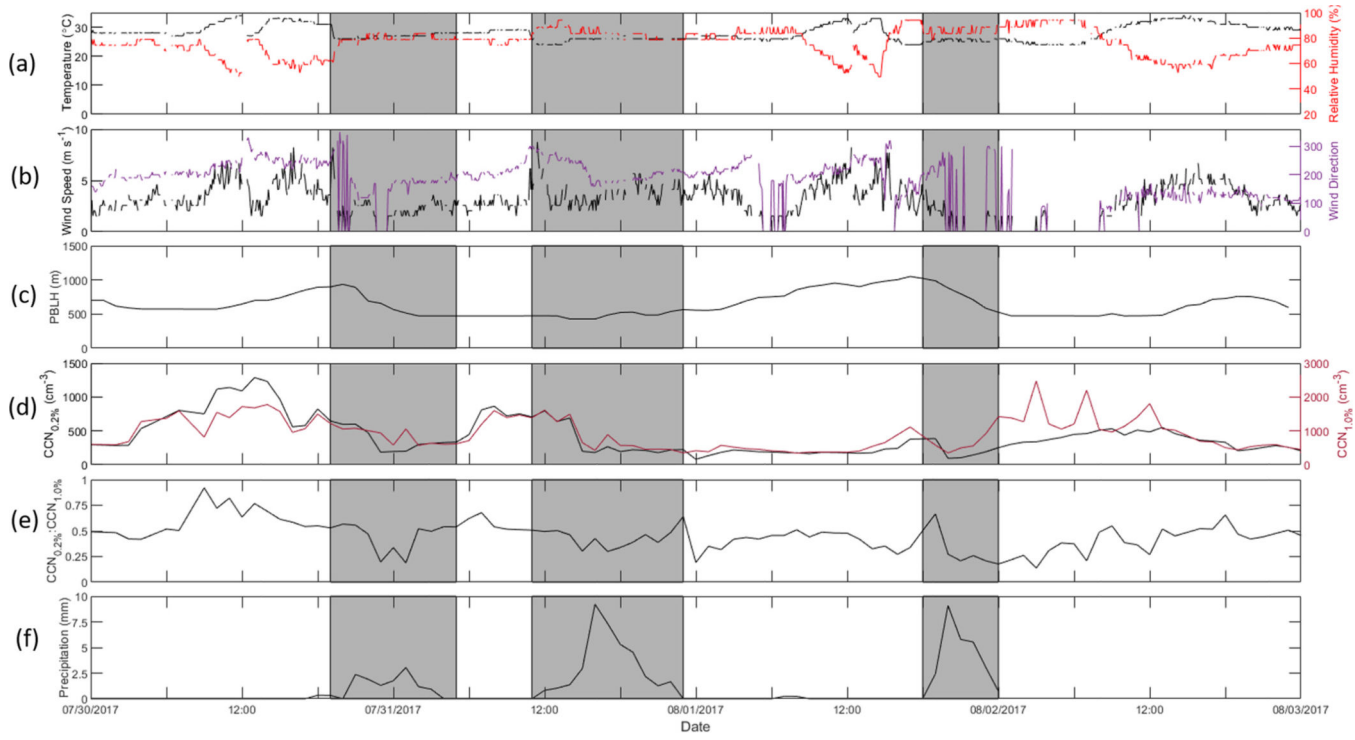

Fig. 10.

Time series of the (**a**) temperature and RH, (**b**) near-surface wind speed and near-surface wind direction, (**c**) PBLH, (**d**) $CCN_{0.2\%}$ and $CCN_{1.0\%}$, (**e**) ratio of $CCN_{0.2\%}$:$CCN_{1.0\%}$, and (**f**) hourly precipitation rates from July 30, 2017 to August 03, 2017. The lines in the plots correspond to the variable written in the same colored font on either the left or right y-axis. The three regions shaded in grey indicate periods in which substantial rainfall occurred.

Table 1

Summary of datasets used in this study.

Data Type	Measurement	Units	Temporal Resolution	Location	Coordinates	Dates Used	Reference
CCN counter	CCN # concentration	cm^{-3}	1 Hz	South Florida's Cloud-Aerosol-Rain Observatory (CAROb)	25.75° N, 80.25° W	Mar–Sep 2013 Jul–Sep 2017 Apr–Jun 2018	Roberts and Nenes (2005)
W-41 filters	Bulk dust mass concentration	$\mu g\ m^{-3}$	Daily*	CAROb	25.75° N, 80.25° W	All months in 2013, 2017, and 2018	Zuidema et al. (2019)
MPL	Depolarization ratio	N/A	Continuous	CAROb	25.75° N, 80.25° W	Jul–Aug 2017	Delgadillo et al. (2018)
IMPROVE	$PM_{2.5}$ speciation and PM_{coarse}	$\mu g\ m^{-3}$	24-h sample every 3rd day	Everglades National Park (ENP)	25.39° N, 80.68° W	All months in 2013, 2017, and 2018	Chow et al. (2015) Hand et al. (2012)
NADP/NTN	Ion mass concentrations in wet deposition	$mg\ L^{-1}$	Weekly	ENP	25.39° N, 80.68° W	Jun–Aug 2017	Gartman (2017)
PERSIANN	Rainfall	mm	3-h and daily	N/A	25.75° N, 80.25° W	All months in 2013, 2017, and 2018	Nguyen et al. (2019)
MesoWest	Temperature Relative humidity (RH) Boundary-layer wind speed Boundary-layer wind direction	°C % $m\ s^{-1}$ ° from north	5-min	Miami International Airport	25.79° N, 80.32° W	July–Aug 2017 Apr 2018	Horel et al. (2002)
NAAPS	Dust and smoke surface concentrations	$\mu g\ m^{-3}$	6-h	N/A	0° to 30°N, 105° W to 45° W	Mar–Jun 2013 Jul–Sep 2017 Apr 2018	Hogan et al. (2014)
MERRA-2	Dust and organic carbon column mass density	$kg\ m^{-2}$	Hourly	N/A	10° to 50°N, 50° E to 140° W	Mar–Jun 2013 Jul–Sep 2017 Apr 2018	Gelaro et al. (2017)
	Planetary boundary layer height (PBLH)	m	Hourly	N/A	25.5° to 26.0° N, 80° W	July–Aug 2017 Apr 2018	Molod et al. (2019)
HYSPLIT	Air mass back trajectories	N/A	12-h	N/A	25.75° N, 80.25° W	Mar–Jun 2013 Jul–Sep 2017 Apr 2018	Rolph et al. (2017) Stein et al. (2015)

*Dust filter sampling can occur daily at south Florida's Cloud-Aerosol-Rain Observatory (CAROb), but is dependent on wind direction and wind speed. Inclusion in the final dataset is dependent on the criteria that the sampling time exceeded 10% of the total available time (e.g., 2.4 h day^{-1}).

Table 2

Criteria used in determining specific days having the most influence from smoke and dust, as well as background days. Days categorized as “other” in this study are all remaining days not covered by the other three categories. Days were only placed in a category if CCN data were available for that particular day.

Day Classification	Dates	Criteria
Dust	Jul 23, 2017 Jul 26, 2017 Aug 04, 2017 Sep 03, 2017	Dust from east (45°–202°) > 96th percentile NAAPS, MERRA-2, and MPL used to verify presence of African dust
Smoke	Mar 02, 2013 Mar 08, 2013 Mar 14, 2013 Mar 29, 2013 Apr 20, 2018	IMPROVE OC and EC > 93rd and 94th percentile, respectively NAAPS and MERRA-2 used to verify presence of smoke
Background	May 04, 2013 Jul 03, 2013 Aug 08, 2013 Aug 23, 2013	IMPROVE OC and EC < 8th and 10th percentile, respectively Dust < 2 μg m^{-3} PERSIANN rainfall < 4 mm NAAPS used to verify absence of smoke and dust

Atmos Environ (1994). Author manuscript; available in PMC 2021 June 30.

Table 3

Average and standard deviation values for the following parameters as a function of the four air type categories: African dust, OC, EC, AmmNit, AmmSul, sea salt, FS, $PM_{2.5}$, PM_{coarse}, daily rainfall, $CCN_{0.2\%}$ and $CCN_{1.0\%}$, and the ratio between $CCN_{0.2\%}$ and $CCN_{1.0\%}$. Values of "N/A" correspond to no available measurements. Average mass fractions (MF) of IMPROVE species in $PM_{2.5}$ are also shown.

		Dust	Smoke	Background	Other
African dust (μg m^{-3})		48.17 ± 18.37	N/A	0.48 ± 0.97	2.54 ± 7.14
OC	(μg m^{-3})	0.41 ± 0.13[a]	1.93 ± 0.68	0.17 ± 0.01	0.51 ± 0.40
	MF	0.07 ± 0.03[a]	0.21 ± 0.08	0.04 ± 0.01	0.10 ± 0.05
EC	(μg m^{-3})	0.04 ± 0.02[a]	0.47 ± 0.12	0.01 ± 0.00	0.10 ± 0.10
	MF	0.01 ± 0.01[a]	0.05 ± 0.01	0.00 ± 0.00	0.02 ± 0.02
AmmNit	(μg m^{-3})	0.38 ± 0.11[a]	0.67 ± 0.21	0.25 ± 0.07	0.39 ± 0.17
	MF	0.06 ± 0.01[a]	0.07 ± 0.01	0.06 ± 0.03	0.08 ± 0.03
AmmSul	(μg m^{-3})	1.56 ± 0.33[a]	2.67 ± 1.02	1.17 ± 0.17	1.80 ± 0.91
	MF	0.25 ± 0.05[a]	0.29 ± 0.11	0.31 ± 0.14	0.33 ± 0.13
Sea salt	(μg m^{-3})	0.80 ± 0.65[a]	0.16 ± 0.05	0.71 ± 0.24	0.67 ± 0.56
	MF	0.11 ± 0.06[a]	0.02 ± 0.00	0.17 ± 0.04	0.13 ± 0.10
FS	(μg m^{-3})	2.50 ± 1.17[a]	1.62 ± 1.19	1.15 ± 1.05	1.45 ± 2.08
	MF	0.36 ± 0.10[a]	0.16 ± 0.10	0.23 ± 0.15	0.20 ± 0.17
$PM_{2.5}$ (μg m^{-3})		6.54 ± 2.34[a]	9.54 ± 1.75	4.26 ± 1.54	5.94 ± 3.16
PM_{coarse} (μg m^{-3})		7.40 ± 3.82[a]	44.51 ± 39.85	6.59 ± 1.74	8.58 ± 7.72
Rain rate (mm day^{-1})		1.23 ± 1.01	0	1.32 ± 1.77	3.45 ± 6.96
$CCN_{0.2\%}$ (cm^{-3})		289 ± 104	1408 ± 976	373 ± 200	343 ± 279
CCN1.0% (cm^{-3})		591 ± 302	3337 ± 1252	584 ± 323	753 ± 564
$CCN_{0.2\%}$:$CCN_{1.0\%}$		0.54 ± 0.17	0.55 ± 0.17	0.71 ± 0.14	0.55 ± 0.21

[a]IMPROVE measurements from EVER1 were unavailable for all dust days. Shown concentrations represent averages for OC, EC, AmmNit, AmmSul, sea salt, FS, $PM_{2.5}$, and PM_{coarse} at EVER1 one day after each dust day. The specific dates used were Jul 24, 2017, Jul 27, 2017, Aug 5, 2017, and Sep 4, 2017.